

**This dissertation has been  
microfilmed exactly as received      68-13,253**

**OLIVER, Jr., George Davis, 1941-  
FAST NEUTRON DOSIMETRY OF CALIFORNIUM-252.**

**The University of Oklahoma, Ph.D., 1968  
Health Sciences, radiology**

**University Microfilms, Inc., Ann Arbor, Michigan**

THE UNIVERSITY OF OKLAHOMA  
GRADUATE COLLEGE

FAST NEUTRON DOSIMETRY OF CALIFORNIUM-252

A DISSERTATION  
SUBMITTED TO THE GRADUATE FACULTY  
in partial fulfillment of the requirements for the  
degree of  
DOCTOR OF PHILOSOPHY

BY  
GEORGE DAVIS OLIVER, JR.  
Norman Oklahoma

1968

FAST NEUTRON DOSIMETRY OF CALIFORNIUM-252

APPROVED BY

Robert Y. Nelson

James W. Smith

Edwin H. Keller

R. A. Howard

C. N. Wright

DISSERTATION COMMITTEE

## ACKNOWLEDGEMENTS

The author wishes to express his appreciation to Dr. R. Y. Nelson for his guidance and encouragement. The suggestions and support from Mr. J. E. Hoy and from the personnel of the Radiological Physics Group at Savannah River Laboratory, Aiken, South Carolina, are acknowledged. The stimulating atmosphere of SRL has been of great service during the performance of this project. I am indebted to my wife, Gayle, with whose considerable forbearance this dissertation was possible. A final note of appreciation is due the Atomic Energy Commission and its contractor, Oak Ridge Associated Universities, Inc., for providing me with an Oak Ridge Graduate Fellowship for the past year and Savannah River Laboratories, operated by E. I. du Pont de Nemours and Company, for providing me with the facilities. This work was done in partial fulfillment of the requirements for the degree of Doctor of Philosophy from the University of Oklahoma.

## TABLE OF CONTENTS

	Page
LIST OF TABLES .....	v
LIST OF ILLUSTRATIONS .....	vi
Chapter	
I. INTRODUCTION .....	1
II. PRINCIPLE OF MEASUREMENT OF FAST NEUTRON DOSE .....	7
A. General Principles	
B. Semiconductor Diode Method	
C. Activation Threshold Foil Method	
III. EXPERIMENTAL PROCEDURE .....	25
A. Method of Irradiation	
B. Experimental Conditions	
C. Calibration	
IV. DOSE DISTRIBUTION AROUND A CALIFORNIUM-252 NEEDLE .....	42
A. Results	
1. Central Axis Depth Dose	
2. Isodose Chart	
B. Analysis and Discussion	
1. Central Axis Depth Dose	
2. Isodose Chart	
V. CONCLUSIONS .....	61
APPENDIX A .....	63
APPENDIX B .....	66
LITERATURE CITED .....	71

LIST OF TABLES

Table	Page
1. Neutron Activation Foil Characteristics .....	20
2. Comparison of Neutron Flux Percentage in Three Energy Ranges .....	33
3. Comparison of Weighted Average Dose Conversion Factors .....	33
4. Central Axis Depth Dose and Percentage rms Standard Deviation for Two Dosimetry Systems .....	46

## LIST OF ILLUSTRATIONS

Figure	Page
1. Structure of the Silicon Diode Dosimeter .....	13
2. Differential Cross Sections of Foil System Elements as a Function of Neutron Energy .....	21
3. Outline Diagram Showing Construction of $^{252}\text{Cf}$ Needle .....	26
4. Example Foil Exposure Lay-out Ready for Immersion in Tissue-equivalent Phantom .....	29
5. Example Diode Exposure Lay-out .....	31
6. Energy Spectra of Fission Neutrons from the Health Physics Research Reactor and $^{252}\text{Cf}$ .....	32
7. Absolute Calibration Curve for PH-50 Neutron Dosimeters after Two Hour Ambient Temperature Anneal ..	37
8. Room Temperature Isothermal Anneal of Voltage for PH-50 Neutron Dosimeters .....	38
9. Relation Between Initial Forward Voltage of PH-50 Neutron Dosimeters and the Re-use Factor .....	41
10. Foil Measured Energy Absorption per $\mu\text{g}$ of $^{252}\text{Cf}$ as a Function of Tissue Depth .....	43
11. Comparison of Energy Absorption as a Function of Tissue Depth along the Central Axis of a $^{252}\text{Cf}$ Source ...	44

Figure	Page
12. Fast Neutron Dose Distribution Around a $^{252}\text{Cf}$ Needle .....	47
13. Distribution of the Percentage Deviation from the Average for the Fast Neutron Dose Around a $^{252}\text{Cf}$ Needle .....	48
14. Longitudinal Distribution of Dose from a $^{252}\text{Cf}$ Needle (Diode Measurements) .....	49
15. Fast Neutron Isodose Chart for a $^{252}\text{Cf}$ Needle .....	50
16. Geometry of Exposure for the Line Source and Detector .....	51
17. Exponential Fits of Depth Dose Data as a Function of Tissue Depth Showing the Depth Dependence .....	53
18. Relative Neutron Dose Percentage Change as a Function of Tissue Depth with Neutron Energy as the Parameter .....	56
19. Simultaneous Plot of KERMA/Fluence and Relative $^{252}\text{Cf}$ Fission Neutron Spectrum As a Function of Neutron Energy .....	64

# FAST NEUTRON DOSIMETRY OF CALIFORNIUM-252

## CHAPTER I

### INTRODUCTION

One of the outstanding applications for radioactivity is radiotherapy. In many forms of human cancer, treatment with ionizing radiation may result in destruction of the neoplastic growth. Since the discovery of radioactivity, x- and  $\gamma$ -rays have been used in every conceivable way to treat all types of cancer. Radium has emerged as the most widely utilized radioisotope, especially for interstitial and intracavity implantation. Although the bulk of clinical knowledge about implant radiotherapy was derived from the use of radium, this material has many disadvantages. Its complex decay series of radioactive daughter products produces gamma-rays with a variety of energies, which complicate dosimetry and prognosis of tissue response. The first daughter, radon, is a radioactive gas and is easily dispersed because it is chemically inert. Thus, the hazard of contamination is prominent in the handling and use of radium. Henschke recently pointed out that radium is the least safe of all medicinal radionuclides in cases of containment rupture.<sup>1</sup> As a result radium spills and releases have caused many costly and embarrassing

cleanup operations.

Not only does radium present serious safety problems, but its radiation type is unsuitable for efficacious treatment "in situ". The high energy radium gamma radiation has great penetration thru tissue. Consequently, an implantation could irradiate too large a volume causing unnecessary death to healthy tissue in proximity to the tumor area. Restriction of volume irradiated raises the probability of effective neoplastic cell kill. The low penetration capability of high energy neutrons corresponds to high energy deposition within the tissue molecules. This dose localization is important because the maximum dose delivered to the tumor cells is limited by the dose received by normal cells near the tumor.

Other sources, such as gold-198, iridium-192, cesium-137, and tantalum-182, have been suggested as suitable substitutes for radium. The use of these isotopes, however, still relies on the relatively penetrating x- and  $\gamma$ -radiation. A possible solution to improved treatment may lie in the application of heavily ionizing particles. Such particles are available only in beams, but would have sufficient energy to deposit maximum energy at the tumor region (Bragg-peak effect).<sup>2</sup>

Schwartz<sup>6</sup> points out that irradiation by heavy ion beams has three significant aspects:

- (1) The deep-seated tumor can be treated more efficiently by permitting delivery of optimal dosage levels to the

tumor site while minimizing the fringe dose to healthy tissue;

- (2) The depth dose and therapeutic ratio (ratio of the tumor lethal dose and normal tolerance dose) can be improved since at superficial depths there is a low linear energy transfer (LET) and a low relative biological effectiveness (RBE), but at interior depths as the Bragg-peak is approached the RBE is relatively large;
- (3) In the relatively anoxic tumor tissue, a low oxygen enhancement ratio (OER) is achieved by high LET particles penetrating to significant depths.

Other theoretical advantages have been proposed and some feasibility studies are in progress for use of deuteron<sup>4</sup>, proton<sup>5</sup>, and  $\pi$ -meson<sup>6</sup> beams. The first two have geometrical advantages rather than biological; the third has biological advantages but has a problem of production in quantity.

Neutrons then are the next logical selection.

Shortly after the discovery of the neutron in 1932 by Chadwick, the possibility of its therapeutic use was recognized.<sup>7</sup> During the past thirty years, however, consideration of neutron beam application was discouraged due to lack of knowledge about neutron damage effects on tissue<sup>8</sup> and the inaccessibility and high cost of available neutron sources. Even recently little importance was attached to the use of a thermal neutron beam in treatment because its attenuation in tissue is too rapid.<sup>9</sup> Increasing the relative number of

epithermal neutrons in a beam increased penetration, but this modification was only as effective at about three cms depth as the thermal neutron beam was at the tissue surface.<sup>10</sup> Due to these considerations it is understandable that the successful techniques in use today employ only x-,  $\gamma$ -, and  $\beta$ -rays. The disadvantages of neutron therapy may be eliminated and techniques made more flexible by using a capsulated source of fast neutrons as an intracavity or interstitial implantation.

The recent availability of transuranic elements, which undergo spontaneous fission, has promoted the development of a unique neutron source. Capsulated californium-252 neutron sources--developed at the Savannah River Laboratory, Aiken, South Carolina--have the advantages of reliability, convenience, availability, and economy.<sup>11</sup> Milligram quantities of this radioisotope are available now; but several grams may be accessible to industry, medicine, research, and education by the 1970's. Californium-252 is more practical than conventional isotopic neutron sources due to its intense neutron emission, ease of fabrication with variable geometries, small volume, reasonable half-life, and low heat emission.<sup>12</sup> With the advent of these small, self-contained sources, "in vivo" neutron irradiation has become feasible.

Utilizing fast neutrons in radiotherapy has several theoretical advantages over conventional radiation:

- (1) smaller depth dose,
- (2) decreased oxygen-enhancement-ratio,

- (3) greater RBE thru increased energy deposition in a cell,
- (4) greater RBE with dose fractionation,
- (5) greater inhibition of tumor recurrence,
- (6) greater absorption in tissues with hydrogen (fatty tumors).

Using a fast neutron beam, instead of a 250 kvp x-ray beam, would be equivalent to an increase of dose by a factor of 1.7, specifically to less oxygenated cells without an increase of dose to healthy cells in the treated region.<sup>14</sup> Having neutrons originate from within a tumor, as in an implant, decreases the dose to healthy tissue and damages primarily the cancerous cells at their site. An interstitial implant, compared with the dose contributed by six collimated beams, would reduce by a factor of ten the neutron dose to healthy tissue.<sup>15</sup> Thus an increased dose to the tumor, effecting a larger kill, would increase the probability of cure.

Evidently, a self-contained, radioactive, neutron source may have advantages that outweigh any disadvantages for radiotherapeutic applications. Now three problems face the therapists: first, estimation of the advantage that fast neutrons may have in treatment of cancer as compared to  $\gamma$ - and x-rays; second, development of a practical scheme of dose measurement; third, determination of the fractionation required to obtain optimum treatment. As Paterson and Parker<sup>16</sup> pointed out, the clinician requires a system of dosage that provides the answers to two questions--what quantity of radiation is required to

produce a particular effect and what is the best distribution of the dose for this effect.

The purpose of this investigation was to describe the fast neutron dose rate in millirad per hour around a linear  $^{252}\text{Cf}$  source in a simulated tissue environment using a practical dosimetry system. Two methods of measurement were used to determine the dose rate decrease with increasing tissue depth--silicon diode dosimeters and activation threshold foils. In addition, the diode dosimeters were used to measure the fast neutron dose distribution in a single plane of  $18\text{ cm}^2$  area around the  $^{252}\text{Cf}$  source. Based on this distribution, an isodose chart was established. Thus, one step has been taken toward the practical application of  $^{252}\text{Cf}$  to radiation therapy.

## CHAPTER II

### PRINCIPLE OF MEASUREMENT OF FAST NEUTRON DOSE

#### General Principles

Further development of radiation therapy requires investigation and exploitation of radio-physical principles. Surface applicators and implants involve very small distances between the sources and the sites of interest in the target volume. As a result, high dose gradients are encountered so that dose specification is difficult.<sup>17</sup> The problem of dosimetry of a spectrum of neutrons, such as those emitted by  $^{252}\text{Cf}$ , must be solved before useful application of the nuclide as a source for radiobiology or medical technology is possible. Neutron fluence rate, energy spectrum, and angular distribution give a fundamental description of the neutron radiation field. From these basics, physical dose can be determined.

A macroscopic measure of interaction is best described as the energy imparted per unit mass of material. The first collisions of the primary particles with nuclei or electrons are based on the scattering cross section. The secondary charged particles produced transfer their kinetic energy to the material by way of excitation and ionization of molecules.

First collision dose for neutrons, then, is the transfer of energy from primary uncharged particles to secondary charged particles within a small volume element. A general term covering this process is the KERMA. If complete charged particle equilibrium exists or if the detector is so small that a negligible part of the energy absorbed results from direct interaction of the primary radiation, KERMA values roughly equal absorbed dose values. In the situation of fast neutrons incident on tissue, the mean free paths of the neutrons are much greater than the ranges of the heavy secondary charged particles, which are mainly protons. For the exposure conditions of this study, charged particle equilibrium can be assumed at any point.<sup>18</sup>

For neutron monitoring, it is possible to obtain dose by several methods.<sup>19</sup> Derivation of dose from neutron fluence depends only on a knowledge of the KERMA/fluence relation and the neutron energy spectrum. NBS Handbook 75 tabulates the first collision dose, or more properly KERMA, for elastic scattering processes in tissue due to fast neutrons. Recently, more accurate revisions of the calculations were published.<sup>20</sup> The revised curves of KERMA vs. neutron energy from 0.1 to 10.0 MeV include consideration of new elastic scattering cross-section data, of angular distribution data, of nonisotropic as well as isotropic scattering data, and of the I.C.R.P. "Standard Man"<sup>21</sup> composition. The revised KERMA data for standard man are similar to those presented earlier, except

for a slight divergence above 3 MeV.

The two techniques used in this experiment, silicon diodes and activation threshold foils, are fluence measuring devices. Although the relative flux distribution of  $^{252}\text{Cf}$  neutrons above 0.1 MeV changes with increasing distance from the source into the phantom material, the dose equivalent does not change appreciably.<sup>23</sup> So an unmoderated  $^{252}\text{Cf}$  fission distribution was assumed present at any point considered. The measured neutron flux was correlated to an equivalent energy deposition in a gram of material by multiplying the neutron spectrum actually entering that gram by the KERMA/fluence relationship (revised). This was an underestimate, but nevertheless a good approximation, of the total neutron absorbed dose.

The energy deposition of a neutron in tissue is complicated by a variety of interactions possible, by large changes in the interaction cross section with energy, and by variations of RBE associated with the charged particles. A complete analysis of the several interaction processes of neutrons with a hydrogenous material is presented by Bethe.<sup>22</sup> For neutrons of thermal or intermediate (0.5 eV to 10 keV) energy, most of the dose is imparted in the process of neutron absorption. The principle interactions are the  $^1\text{H}(n, \gamma)^2\text{H}$  and  $^{14}\text{N}(n, p)^{14}\text{C}$  reactions. They contribute 10-15% of the total dose, depending on the depth of tissue irradiated and consequently on the average incident neutron energy.<sup>23</sup>

At depths greater than three cms, build-up of absorbed dose from the hydrogen capture  $\gamma$ -rays becomes prominent. But this is probably insignificant compared to the fission product gamma-ray dose.<sup>10</sup> Fast neutrons interacting with low atomic number materials--especially hydrogen--in tissue account for 80 to 90% of the total absorbed dose. This is true because the hydrogen atoms are more abundant and a large average fraction of the energy lost in an elastic collision is dissipated by the lighter atoms. For beams of  $\bar{E} \geq 0.5$  MeV the contribution of the thermal dose is negligible, but is of increasing importance as the average neutron energy of the beam decreases.<sup>24</sup>

One of the assumptions made for irradiation was that a patient is a homogeneous volume of tissue. It is realized though that a patient has a heterogeneous composition, and such doses obtained under this assumption are only good approximations. The usual corrections, applied for extra absorption in bone or extra transmission in the lung, for the curvature of surfaces encountered by the beam, or for the fact that part of the body being treated is much smaller than the phantom in which the basic data was measured, are unnecessary.

Neutron fluence may be measured using devices which:

- (1) have high neutron sensitivity,
- (2) have gamma-ray insensitivity,
- (3) are small enough in volume to prevent considerable

disturbance of the radiation field,

- (4) are thin enough to insure that the probability of two collisions by a single neutron with the material is small but thick enough compared to the ranges of secondary charged particles produced.

Primarily two types of devices meet these criteria--silicon semiconductor dosimeters and activation threshold foils.

#### Semiconductor Diode Method

The semiconductor neutron dosimeter is a silicon junction diode which can determine the integrated fast neutron fluence incident upon it.<sup>25,26</sup> The wide base, conductivity-modulated, n<sup>+</sup>-p-p<sup>+</sup> device changes electrical characteristics in a manner which is proportional to the incident neutron fluence and corresponding integral dose. A 50 mils base width diode responds to a range of dose from 10-1000 rads. The small volume, gamma-ray and thermal neutron insensitivity, ruggedness, and permanency of dose related characteristic changes make these devices particularly convenient to use in radiobiological applications. Conversion of the fluence value to an integral KERMA is straightforward. The few disadvantages associated include temperature sensitivity, non-linear energy dependence, and slight annealing of the neutron-induced changes.

The diodes are made of 50 ohm-cm, low-oxygen silicon in disk shape with two nickel end terminals for electrical contacts. The silicon base width (d) is 50 mils and its diameter

is 120 mils. A high resistivity material was selected to provide a high carrier lifetime and a low carrier concentration in the base. Phosphorus is diffused on one face to form the n<sup>+</sup>-p junction and boron is diffused on the other for the p<sup>+</sup>-p junction. The (+) indicates a superdoping level exceeding  $10^{18}$  atoms per cubic centimeter. A side view of the diode structure is presented in Figure 1.<sup>26</sup>

Irradiating this silicon semiconductor with fast neutrons causes lattice dislocations in its crystal structure, due to elastic and inelastic scattering. Permanent recombination centers are formed and, along with chemical impurities, tend to trap excess carriers moving thru the material. Consequently, the diffusion length (L), mobility of the excess carriers ( $\mu$ ), and the excess carrier lifetime ( $\tau$ ) are decreased. These reductions produce a decrease of average injected carrier concentration in the base region and are manifested by an increase of the forward resistance ( $R_f$ ) of the device. A measurement of the change in  $R_f$  is achieved by monitoring the increase in forward voltage ( $V_f$ ) while carrying an optimized, constant current of 100 milliamperes. Calibration curves have been established which relate the forward voltage to an incident fluence of fission spectrum neutrons.<sup>25,27</sup> For the stated range of dose sensitivity (fluences below  $10^{13}$  nvt), the increase in  $V_f$  is due to a decrease in  $\tau$  according to the following relation:

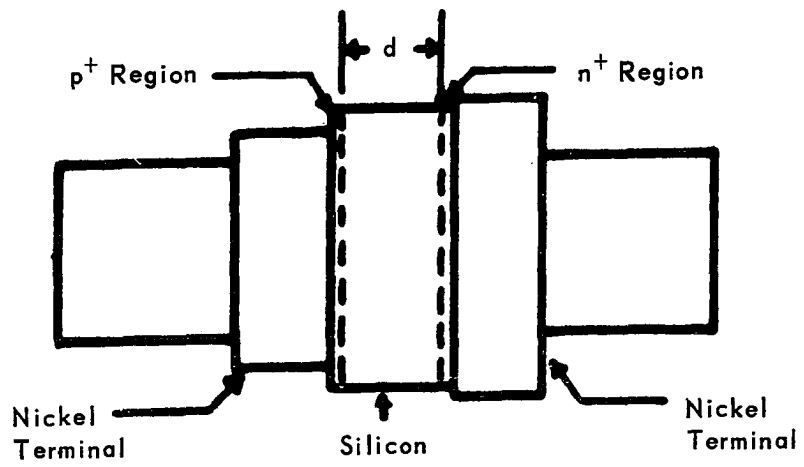


FIG. 1 STRUCTURE OF THE SILICON DIODE DOSIMETER

$$\frac{1}{\tau_f} - \frac{1}{\tau_0} = \alpha \phi,$$

where  $\tau_f$  and  $\tau_0$  are lifetimes after and before irradiation respectively;  $\alpha$  is the effective lifetime damage constant in the base region; and  $\phi$  is the fast neutron fluence. Or

$$\Delta\left(\frac{1}{\tau}\right) = \alpha' D_f$$

where  $D_f$  is the fast neutron dose in rads. Since  $\tau$  is related to  $V_f$ ,

$$\Delta V_f = \beta D_f$$

Thus the effect of a single parameter, carrier lifetime, and its effect on the current-voltage characteristics of the diode enables an ideal correlation to neutron bombardment. A complete discussion and derivation of the previous ideas is presented by Swartz and Thurston.<sup>28</sup>

The sensitivity of the diode is a function of base thickness ( $d$ ) as well as carrier lifetime. The larger  $d$ , the greater the sensitivity is. However, due to fabrication limitations, a threshold exists; a  $d$  of fifty mils gives optimum sensitivity and stability.<sup>25</sup> Such diodes (Model PH-50 from Phylatron Corporation, Columbus, Ohio) have a sensitivity of about 2 mv/rad.<sup>26</sup> The r m s scatter of the measured dose is <5% for doses >50 rads; the precision of measurement decreases with decreasing dose. Better precision and accuracy of measurement would result from development of a more sensitive read-out system with good temperature

compensation and from modification of the device structure.<sup>27</sup> The diodes exhibit no dose rate dependence.

A second and more serious problem is that the  $V_f$  is also a function of temperature. If the diode is stored, exposed, and read-out at a constant temperature (ambient), this problem is minimized.

The response of the device is dependent on the incident neutron energy.<sup>26,29,31</sup> The variation of sensitivity for energies from 0.30 to 5.0 MeV is about  $E_n^{1/3}$  and from 5.0 to 22. MeV is not definitely established. Apparently, the response drops rapidly below 0.20 MeV.

The diodes have discrimination against thermal neutron and gamma-ray radiation. Six diodes were exposed to  $10^8$  nvt in a thermal column beam from a reactor at Savannah River Laboratory which had a cadmium ratio of about 120. No response was detected. An exposure to about 6000 R from a  $^{60}\text{Co}$  source also produced no response.

The isothermal annealing (reordering) properties in the base region of the fifty mils diodes have been investigated.<sup>30</sup> The radiation-induced defects anneal due to two processes: (1) a monomolecular process in which the defect concentration has no dependence on the time dependence of anneal and (2) a bimolecular process in which the defect concentration is dependent on the time dependence of anneal. The structural defects tend to interact with other imperfections, chemical impurities, and dislocations and tend to be nullified.

Changes in measured values are temperature and time dependent. Data from experiments indicate the annealing is governed by the breakup of the individual defect clusters. The first investigations showed an anneal of 10 to 15% from a time two hours after irradiation to a time twelve days later.<sup>27</sup> However, later results showed as much as 30% anneal for the same time interval<sup>30</sup> (see Calibration section). The diodes have a practical lower detection limit of about 10 rads, which makes them too insensitive for use in low-level neutron dosimetry. However, they are relatively inexpensive, are easy to read, are convenient for exposures in complex geometry situations, have an established absolute calibration relation, and are reliable to about  $\pm 10\%$  at 50 rads dose. These semiconductor devices can be used as fast neutron dosimeters by measuring the incident fluence from a known neutron energy spectrum.

#### Activation Threshold Foil Method

The use of activation threshold foils for detection of fast neutron fluence has been common for many years in reactor technology.<sup>32</sup> The basis of the method is that neutrons are allowed to interact with materials of known cross sections and the fluence is determined by measurement of the induced activity. The tissue dose then can be determined by calculation, utilizing the empirical relationship established between neutron fluence and absorbed energy. In other words, the

induced activity in the material is directly proportional to the incident neutron fluence. The first generally accepted division of a spectrum is described by Hurst et. al.<sup>33</sup> This technique has several advantages:

- (1) Threshold materials are insensitive to high gamma-ray fluxes;
- (2) Small volume, availability of materials, and variable geometries allow convenience during exposure and evaluation;
- (3) Materials may be selected for response to neutrons in a desired energy range;
- (4) Activity produced by neutron interaction may easily be related to tissue KERMA.

On the other hand the method has low and varying limits of detectability, large errors present in cross section values, and tedious calculations. Several properties, or requirements, exist for ideal activation monitors in relation to "in phantom" measurements:

- (1) Threshold energies should span the neutron energy region of interest;
- (2) Effective activation cross sections should be well known;
- (3) Daughter product of the material should decay by a single radiation process with a relatively long half-life;
- (4) Detector material should be available with a high purity from trace contaminants;

- (5) Detector material should have low cost and be easily handled;
- (6) Detector material and daughter product should be chemically stable and compatible to the environmental conditions of irradiation.<sup>34</sup>

This method is most useful when prior knowledge of the spectrum is available. For this investigation an unmoderated fission spectrum is assumed. Because of the inaccuracies in cross section values and decay schemes, the derivation of the spectrum at each point of interest would be difficult to derive with any meaningful results. Attempts have been made to mathematically derive the spectrum; but, generally, these are not satisfactory unless they incorporate an assumption of some approximate spectral shape.<sup>35</sup>

Elements useful to neutron activation methods must have either a constant activation cross section over a wide range of energy or a much larger one for a particular range. For an ideal threshold reaction the cross section above some threshold energy  $E_T$  is constant and below is zero. The distribution shape of any actual differential cross section varies considerably. So an effective cross section can be calculated which is an average value above some effective  $E_T$  weighted for a given neutron spectrum (usually a fission spectrum). The true cross section for activation as a function of neutron energy  $\sigma(E)$  can be replaced by a constant, effective cross section  $\sigma_{\text{eff}}$  by the following relation:

$$\sigma_{\text{eff}} = \frac{\int_0^{\infty} \phi(E) \sigma(E) dE}{\int_{E_T}^{\infty} \phi(E) dE}$$

where  $\phi(E)$  is the flux distribution function.<sup>36,37</sup>

The activation threshold foil system used for measurements in this investigation was adapted from the criticality neutron dosimeter described by Wright.<sup>38</sup> The detectors consist of copper for determining the flux from 2.0 eV to 1.0 MeV, indium for determining the flux above 1.0 MeV, and sulfur for determining the flux above 2.5 MeV. The dose can be determined by:

$$D = [1.44 \phi_{\text{Cu}} + 2.88 (\phi_{\text{In}} - \phi_{\text{S}}) + 3.9 \phi_{\text{S}}] \times 10^{-9}$$

where  $D$  is the KERMA times 0.01 rad/ergs/g;  $\phi_{\text{Cu}}$ ,  $\phi_{\text{In}}$ , and  $\phi_{\text{S}}$  are the neutron fluences (n/cm<sup>2</sup>) in their respective energy ranges. The coefficients in the equation are the weighted average KERMA/fluence factor. Appendix A describes the calculations used for their determination. Table 1 presents a few pertinent characteristics of the foil elements. Effective cross section value for the copper (n, $\gamma$ ) reaction is from Anderson<sup>39</sup>, for the indium (n,n') reaction is from Bresesti<sup>40</sup>, and for the sulfur (n,p) reaction is from Reinhardt<sup>36</sup>.

TABLE 1

## Neutron Activation Foil Characteristics

Foil Material	Nuclear Reaction	Effective Cross Section (barns)	Energy Range (MeV)	Product Half-Life
Copper (Cd-clad)	$^{63}\text{Cu}(n,\gamma)^{64}\text{Cu}$ 29	0.258	2.0 eV-1.0	12.8 hr
Indium (Cd-clad)	$^{115}\text{In}(n,n')^{115\text{m}}\text{In}$ 49	0.155	1.0->8.0	4.4 hr
Sulfur	$^{32}\text{S}(n,p)^{32}\text{P}$ 16	0.229	2.5->8.0	14.2 d

The differential cross section for each of the foil elements is presented in Figure 2. The effective cross section with its  $E_T$  is also shown for sulfur.

The following general expression relates the observed counting rate (CPM) of the activated material to the incident neutron flux ( $\phi$  in  $n/\text{cm}^2/\text{min}$ ):

$$\phi = \frac{(\text{CPM})(Q)(\text{CLF})}{(W)(K)(N_T)(\sigma_{\text{eff}})(1-e^{-\lambda T_0})(e^{-\lambda T_1})}$$

where  $Q$  is the counter efficiency factor in d/count,  $CLF$  is the empirical calibration factor in n/d,  $W$  is the foil weight in grams,  $K$  is the natural isotopic abundance,  $N_T$  is the nuclear density in nuclei/gram,  $\lambda$  is the decay constant of the activated isotope in  $\text{min}^{-1}$ ,  $T_0$  is the exposure time in min,  $T_1$  is the time lapse between exposure stop and mid-point

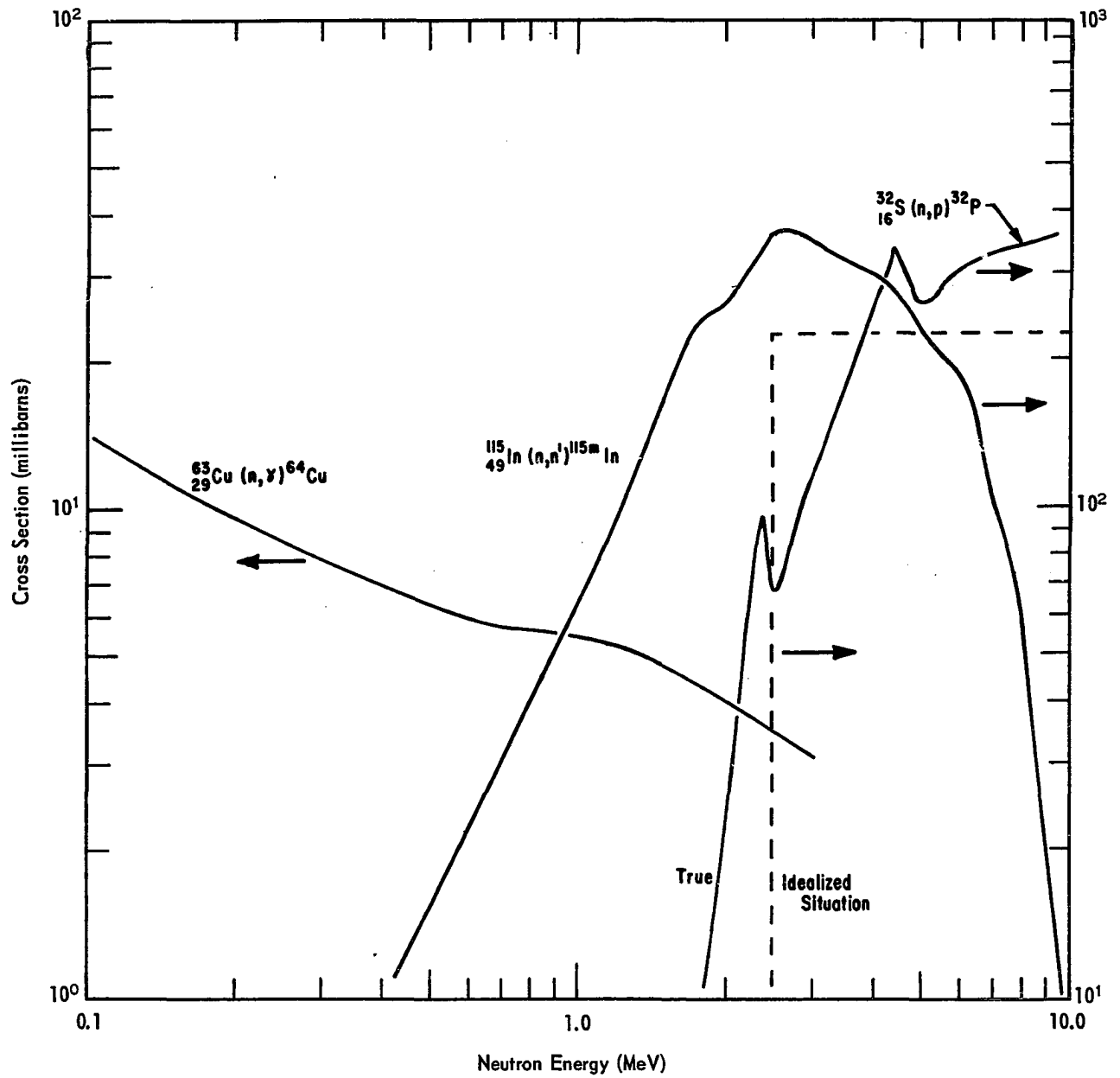


FIG. 2 DIFFERENTIAL CROSS SECTIONS OF FOIL SYSTEM ELEMENTS AS A FUNCTION OF NEUTRON ENERGY

of the counting period in minutes. The CLF accounts for geometry, backscatter, self-absorption in the foil, and absorption in the air, in the window of the counter, and in the foil cover. Appendix B presents the equations and specific values for conversion from CPM to  $\phi$  for each type foil. All constant terms used in calculating the foil measured flux are presented to allow other investigators to draw directly from the technique with a minimum of conversion.

Copper-63 has a response to neutrons with energies ranging from 2 eV to about 1 MeV with a resonance energy peak at 580 eV. The differential cross section approaches 1.0 MeV with a  $1/E$  relation. This range extends much below the assumed cut-off point of 0.10 MeV. However, below this, the contribution of neutrons from the  $^{252}\text{Cf}$  fission spectrum is <1% of the total, and the dose conversion factor is ten times lower than factors above that energy. So a small dose, which is not considered to be in the sensitive range of this system, is included in the copper region dose values. The copper  $(n,\gamma)$  reaction produces  $^{64}\text{Cu}$  which decays by electron capture (42%), positron emission (19%), and negatron emission (39%) at a 12.8 hr half-life. A low level, gas flow, GM-type beta counting system was convenient to detect the copper activation levels. The counter background was 0.6 cpm; and the counter efficiency was 43.4%, based on a  $^{32}\text{P}$  standard. A competing reaction produced  $^{66}\text{Cu}$  (5 minute half-life), but a short wait before counting reduced any interference. To

minimize the response to neutrons below 2 eV, the copper foils were clad with 35 mils thick cadmium. Each foil had a 7/32 inch diameter and was 5 mils thick, exposing about 113.5 mg/cm<sup>2</sup> of material to the incident flux.

Elemental indium is composed of two isotopes--4.2% <sup>113</sup>In and 95.8% <sup>115</sup>In by weight. Both isotopes have a large thermal neutron cross section, which can be eliminated from consideration by covering the indium foil during exposure with 35 mils thick cadmium. Two interactions remain responsive to epi-cadmium neutrons. The inelastic scatter interaction of fast neutrons has a threshold at 0.45 MeV but only becomes significant around 1.0 MeV. The reaction product <sup>115m</sup>In undergoes isomeric transition (95%) and decays to <sup>115</sup>Sn by beta emission (5%) at a 4.4 hr half-life. The capture reaction, which has a resonance above the cadmium cut-off, produces <sup>116m</sup>In. This isomer may decay to <sup>116</sup>Sn by one of three beta modes and a series of gamma-rays at a 54 min half-life. Obviously, gamma spectroscopic methods were required to distinguish the activation level of the desired inelastic scatter reaction. A low level scintillation system with a 9 in NaI well crystal was used to analyze the indium foils. The second section of Appendix B presents a detailed explanation of the analysis procedure. All indium foils were the same size as the copper foils.

Sulfur-32 has a convenient threshold response to fast neutrons with energies >2.5 MeV. The reaction produces <sup>32</sup>P

which decays by simple beta emission with a half-life of 14.3 days. The same low level beta counter used for copper foil counting was used. To increase the probability of interaction in as small a volume as possible the sulfur powder was pressed into pellet form with a density of  $2 \text{ gm/cm}^3$ . Each pellet was  $8/32$  in diameter and was either 115 or 155 mils thick. Preparation for counting involved burning of the sulfur pellet on a counting planchet, leaving the  $^{32}\text{P}$  deposited. The counting sensitivity of this technique increases since a burned sulfur sample gives the same count rate as an unburned sample of zero thickness if all the  $^{32}\text{P}$  is recovered.<sup>36</sup>

Materials which have known differential cross sections can be used to relate induced activity to an incident neutron flux. In turn, this flux can be related to tissue KERMA for a known neutron energy distribution. The three materials sulfur, indium (cadmium-clad), and copper (cadmium-clad) are serviceable to evaluate the flux in three energy ranges above 2.0 eV of a fission spectrum. Properly calibrated, this system is a reasonable fast neutron dosimeter.

## CHAPTER III

### EXPERIMENTAL PROCEDURE

#### Method of Irradiation

As an approximation to the human torso, a right, elliptical cylinder (axis 20 cm x 36 cm; 60 cm tall) was constructed from 0.64 cm polyethylene and filled with a tissue-equivalent (T-E) solution. This solution has the same relative atomic composition as found in average wet human tissue. The compounds used are distilled water, sucrose, and urea, resulting in 10% H, 4% N, 74% O, and 12% C by weight.<sup>41</sup>

The neutrons were obtained from a linear californium-252 source, encapsulated like a cell-loaded radium needle (see Figure 3). The linear source was prepared by uniformly electrodepositing californium hydroxide on a 2.0 cm length of thin platinum-iridium wire. Heating the wire changed the deposition to relatively insoluble californium-oxide. The wire was placed in a platinum cell which was sealed with a silver-soldered cap.<sup>42</sup> A helium leak detector tested the integrity of the cell by exposing it to 30 psi helium for 30 minutes; any leak rate was approximately the lower detectability of the instrument ( $<2 \times 10^{-9}$  cm<sup>3</sup>/sec). The cell was placed in a platinum-iridium sheath with a threaded cap and was silver-soldered shut. Another leak test was performed.

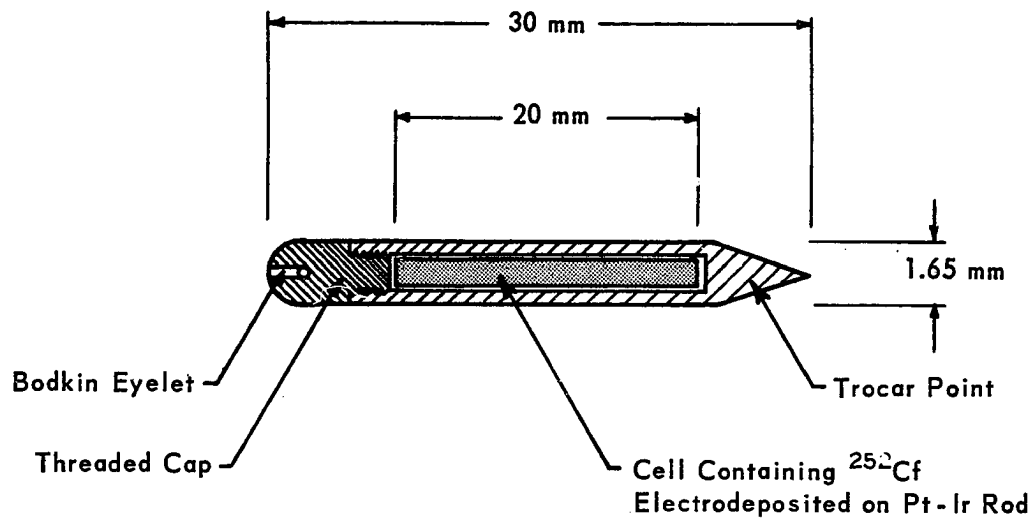


FIG. 3 OUTLINE DIAGRAM SHOWING CONSTRUCTION OF  $^{252}\text{Cf}$  NEEDLE

Calculations show that the cell can withstand the internal pressure buildup from fission product gases and helium from alpha decay.<sup>43</sup>

The neutron source strength was determined using a manganese sulfate bath, which is cross-calibrated with the National Bureau of Standards (NBS) system. The absolute emission rate was  $1.058 \pm 0.012 \times 10^7$  n/sec on August 8, 1967; this corresponds to an equivalent Cf mass of  $4.529 \pm 0.04$   $\mu$ g. Due to the presence of a 1.1% contamination of  $^{254}\text{Cf}$  in the source material for the  $^{252}\text{Cf}$  needle, the effective half-life of 2.55 yrs was not present. Successive absolute neutron emission calibrations, made with the manganese sulfate bath, indicate a shorter initial half-life. All dose measurements are normalized to correspond to the source strength on the day these experiments were initiated.

Since  $^{252}\text{Cf}$  undergoes spontaneous fission, a typical fission neutron spectrum is produced with neutron energies ranging from 0.003 to 15.0 MeV. The portion of neutrons above 7.5 MeV is of such low prevalence that its contribution to the total fast neutron dose is insignificant for this study. The energy spectrum is described by the empirical expression  $N(E) \propto e^{-0.88E} \text{SINH} \left[ (2.0E)^{\frac{1}{2}} \right]$ , where  $N(E)$  is the number of neutrons of energy  $E$  per unit energy.<sup>44</sup> The average neutron energy ( $\bar{E}_n$ ) is 2.34 MeV and the most probable neutron energy is about 0.7 MeV. Fields and Diamond present a complete review of  $^{252}\text{Cf}$  as a neutron source.<sup>45</sup>

### Experimental Conditions

The dose rate drop-off in a plane perpendicular to the central axis of the source was measured at 0.5 cm intervals to a distance of 4.0 cm. The centers of the dosimeters and the center of the source were adjusted to be in a plane. A plexiglas sheet (0.32 cm x 10 cm x 15 cm) provided a constant, reproducible geometry with a machined groove for the needle and with holes for the diodes or slots for the foils. Comparative dose measurements made with and without the supporting material agreed within the experimental error, showing that the plexiglas had no observable difference in neutron absorption properties from that of the solution. A typical exposure geometry for the two systems is exemplified by the foil lay-out pictured with the phantom in Figure 4.

Exposure times varied from 5 to 60 hrs, depending on the distance from the needle. The cross sectional area of the foils was about 0.242 cm<sup>2</sup> and of the diodes was about 0.04 cm<sup>2</sup>. Optimum geometry for a point detector required a smaller foil area, but enough material was needed to produce an activation level above that required for the minimum counting sensitivity.

Both systems of dosimeters were compared by measuring the same dose drop-off. If they agreed, the simpler and quicker diode system then could be used to determine the dose rates on a 0.5 cm grid over an 18 cm<sup>2</sup> area around the needle. The source was assumed to have isotropic emission, allowing measurements on either half of the chosen plane around the

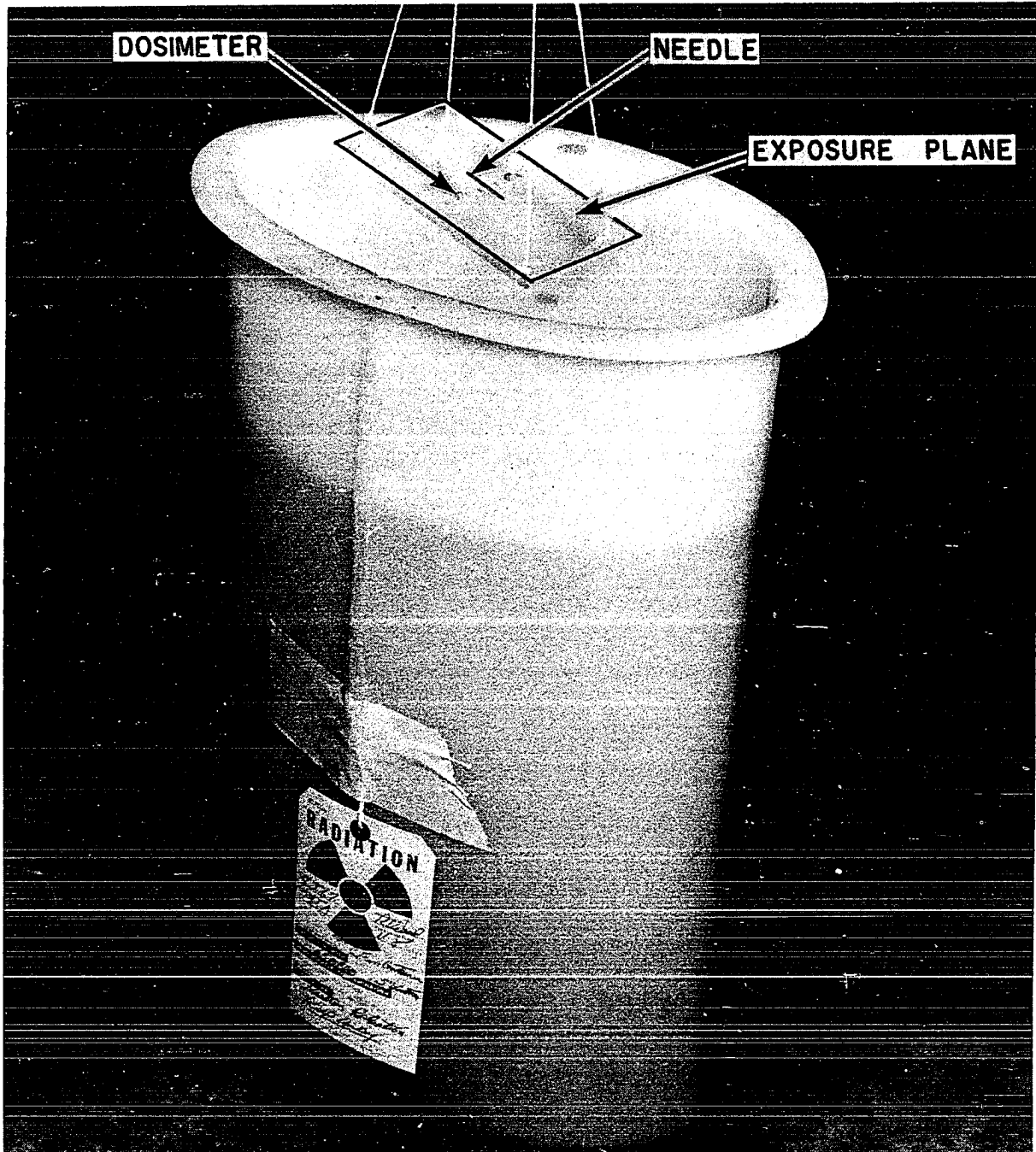


FIG. 4 EXAMPLE FOIL EXPOSURE LAY-OUT READY FOR IMMERSION IN TISSUE-EQUIVALENT PHANTOM

needle. Dose rates were measured at 78 points with 4 to 8 runs per point. A typical planar exposure arrangement for the diodes is shown in Figure 5. By appropriate interpolation of dose rates on the grid, isodose lines were drawn. Such lines indicate the contour variation of the dose pattern over the area adjacent to the source.

### Calibration

Since absolute as well as relative results were desired, a calibration of the two dosimetry systems was required. The Health Physics Research Reactor (HPRR) at the Oak Ridge National Laboratory DOSAR Facility was chosen as a neutron calibration source because it has a well-known neutron spectrum shape and its personnel have made successful advances to have it accepted as a national and international intercomparison standard for dosimetry systems.<sup>46</sup> This reactor is a small, unshielded and uncooled, fast reactor of the Godiva type.<sup>41</sup> A comparison of the HPRR and californium unmoderated neutron energy spectra is shown in Figure 6.<sup>45,48</sup> The percentage of total flux in the three ranges considered by the threshold materials is shown in Table 2 for both spectra.

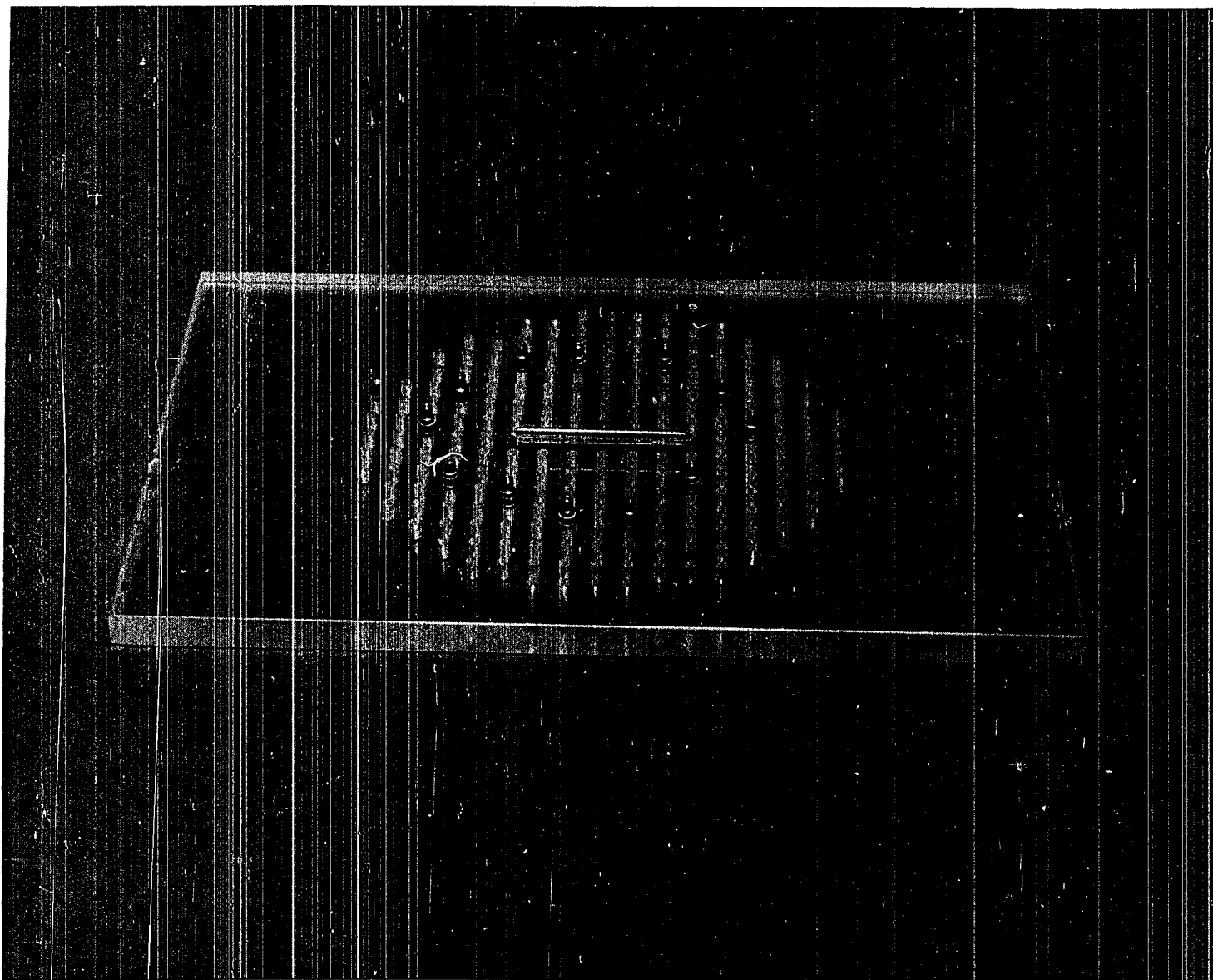


FIG. 5 EXAMPLE DIODE EXPOSURE LAY-OUT

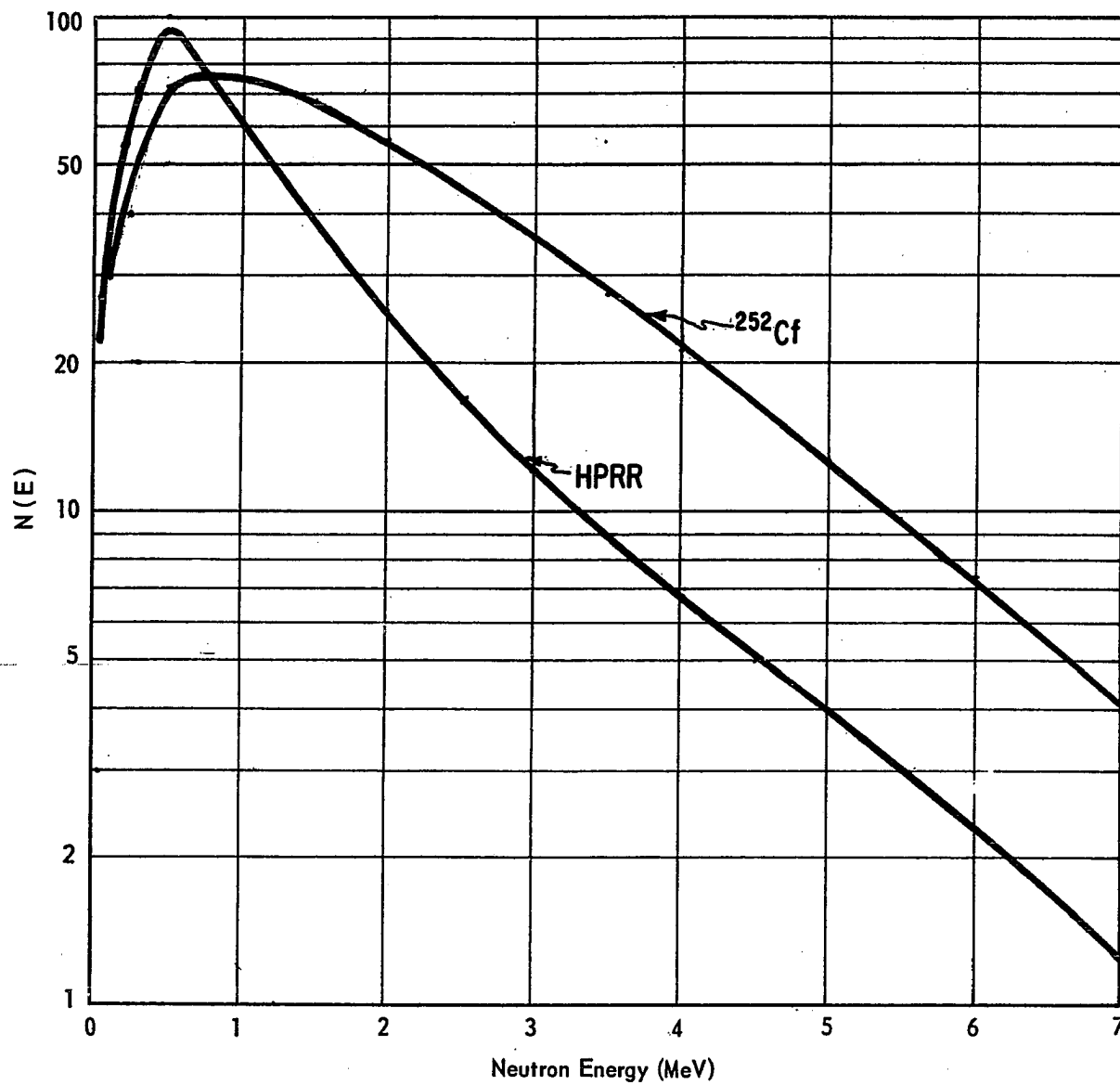


FIG. 6 ENERGY SPECTRA OF FISSION NEUTRONS FROM THE HEALTH PHYSICS RESEARCH REACTOR AND  $^{252}\text{Cf}$

TABLE 2

Comparison of Neutron Flux Percentage in Three Energy Ranges

Spectrum	Energy Range		
	0.1-1.0 MeV	1.0-2.5 MeV	2.5 MeV up
Californium-252	25.9%	39.5	34.6
HPRR	46.9	35.1	18.0

Although the spectra are different in shape and average energy, the weighted average dose conversion factors are approximately the same (see Table 3). Appendix A presents a derivation of these factors.

TABLE 3

Comparison of Weighted Average Dose Conversion Factors

Spectrum	Energy Range		
	0.1-1.0 MeV	1.0-2.5 MeV	2.5 MeV up
Californium-252	$1.44 \times 10^{-9}$ rad/n/cm <sup>2</sup>	2.88	3.90
HPRR	1.50	2.80	3.97

On October 25, 1967, the two dosimetry systems were exposed in air to HPRR for a sixty minute run at 175 watts,

producing a neutron flux above 100 KeV of  $6.24 \times 10^{10}$  n/cm<sup>2</sup>. Computed in accord with the HPRR spectrum, this flux implied a dose of  $163.3 \pm 6.2$  rads at 2.0 m and 72.6 rads at 3.0 m. The accepted primary source for this dose is the initial count rate (ICR) of the activation sulfur pellet established by DOSAR as the normalization channel.<sup>49</sup> Calibration was empirical so the accuracy of the investigation depends on the exactness of the neutron dose values obtained from DOSAR. A long run rather than a burst was used to approximate actual exposure situations. The reactor height and detector height were 2.0 m above the floor of the reactor room.

The purposes for calibration were threefold: (1) to derive calibration factors for the geometries of the foil system, (2) to test the accuracy of the read-out system using the absolute diode voltage response curve, (3) to establish a relationship between the initial forward voltage  $V_f)_i$  and the diode re-use factor (R). For calibration, the foil system consisted of six copper and six indium, cadmium-clad, foils and twelve sulfur pellets. Except for the sulfur, the system was identical to that used for the Cf dose measurements. An average fluence of  $2.12 \times 10^9$  d/cm<sup>2</sup> was computed for the copper foils; dividing this into the known fluence in the copper region of the energy spectrum,  $3.19 \times 10^{10}$  n/cm<sup>2</sup>, the copper calibration factor (CLFC) is 1.51 neutrons/disintegration. The ratio for indium foils (CLFG) is 1.50 neutrons/count. Since a secondary standard of phosphorus-32

was obtained, the counter efficiency factor ( $d/c$ ) was known for the sulfur samples. The similar ratio for sulfur (CLFS) is  $0.80 n/d$ . As stated in Chapter II, two thicknesses of sulfur pellet were used for the dose evaluation close to the californium needle. Consequently, fourteen pellets, ranging in thickness from 75-279 mils, were included in the calibration to determine if there was any effect on the activation, or subsequent counting, due to pellet thickness. Comparison of disintegrations per minute per gram (dpm/g) with pellet thickness (mils) revealed that all data fell within a standard deviation of 8.0% at the 95% confidence level. Certainly, little change of response existed between the 155 mils and 115 mils thick pellets.

Forty-one diodes were calibrated at ambient temperature. The resulting increase of  $V_f$  was used to calibrate the read-out system and establish a relationship for the re-use factor as a function of initial  $V_f$ . Kramer<sup>25</sup> and Thurston et. al.<sup>26</sup> had already established an absolute calibration curve for the response of the PH-50 type diodes (at  $V_f = 1.00$  volt) with neutron dose by exposing them to fast neutron bursts from several reactor facilities. They checked system calibration at high dose levels at the Sandia Pulsed Reactor Facility, DOSAR, Ohio State University Research Reactor, and Battelle Research Reactor. Additional low dose sensitivity with long exposure times was determined with a PuBe, secondary standard, neutron source.<sup>26</sup> Diodes having low  $V_f)_i$  ( $<1.000$  volts) were

especially considered for response. A Watt fission spectrum was assumed for conversion of the measured neutron flux to dose. Then all calibrations were averaged and re-adjusted to conform to the fast neutron dosimetry used at DOSAR. The PH-50 average calibration curve (Figure 7, after two hour ambient temperature anneal) was accepted as the correct absolute response curve.<sup>27</sup> For maximum accuracy each diode should be individually calibrated to account for its inherent variations. But a calibration exposure would destroy the virgin properties of the device. Since the interaction process, which produces the change in electrical characteristics, is a statistical one, a spread of response with an acceptable average response is expected. According to Chase et. al.<sup>27</sup>, these dosimeters measure fast neutron doses to accuracies of  $\pm 10\%$  and have a relative r.m.s. deviation between individual dosimeters not greater than 10% in a dose range from 5-500 rads. The SNDR-2 diode reader (designed and built by Phylatron Corporation, Columbus, Ohio) was calibrated within  $\pm 0.5\%$  against a secondary standard voltmeter for conditions of read-out, i.e. 100 milliamperes constant current with full scale voltage of 2.5 volts.

Periodic measurements of the isothermal decrease of the  $V_f$  were made on the forty-one diodes over a 450 hour interval. The effect of room temperature regeneration processes is shown in Figure 8 as percentage  $V_f$ )<sub>2 hr unannealed</sub> versus time after exposure. The ordinate is calculated as the ratio

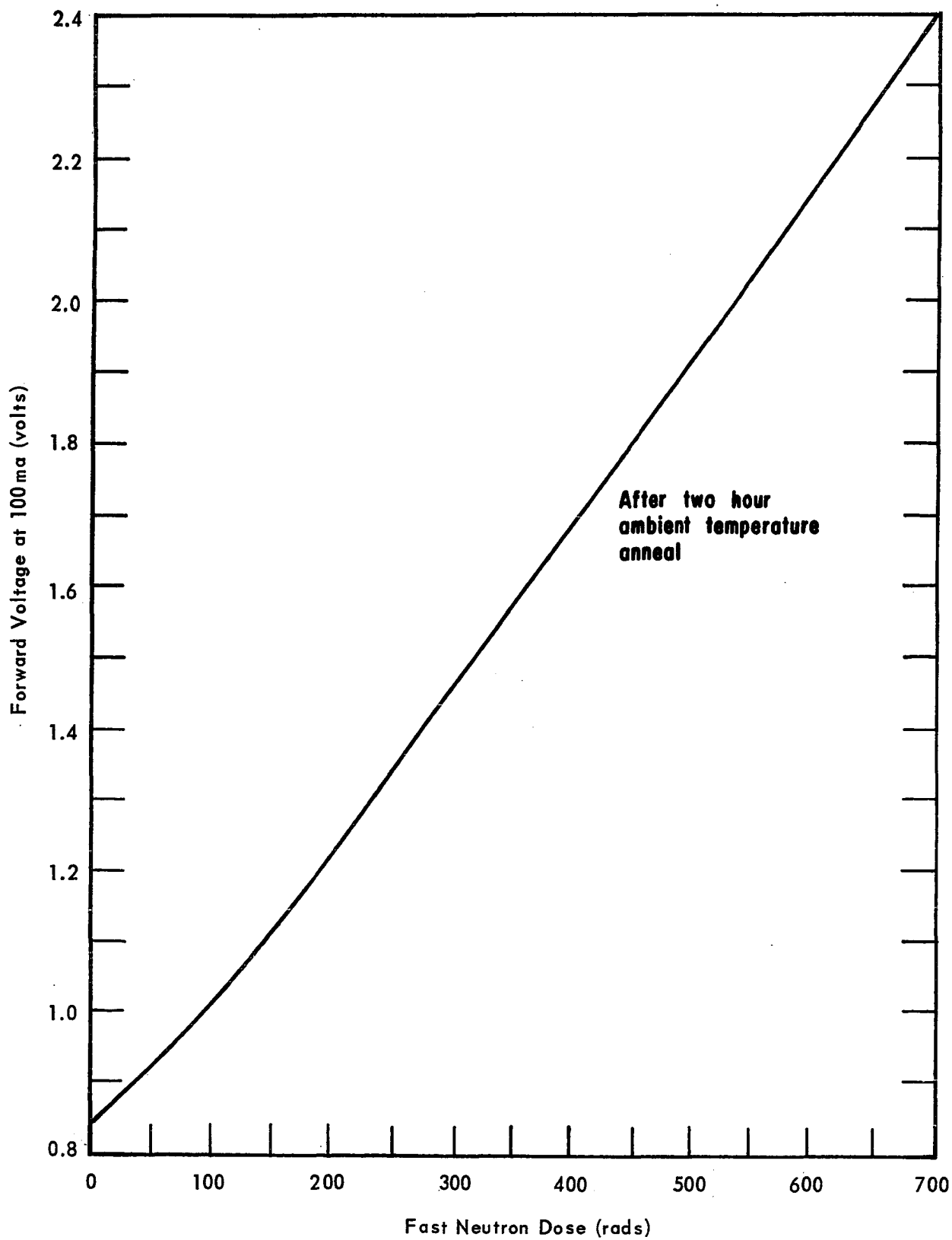


FIG. 7 ABSOLUTE CALIBRATION CURVE FOR PH-50 NEUTRON DOSIMETERS AFTER TWO HOUR AMBIENT TEMPERATURE ANNEAL

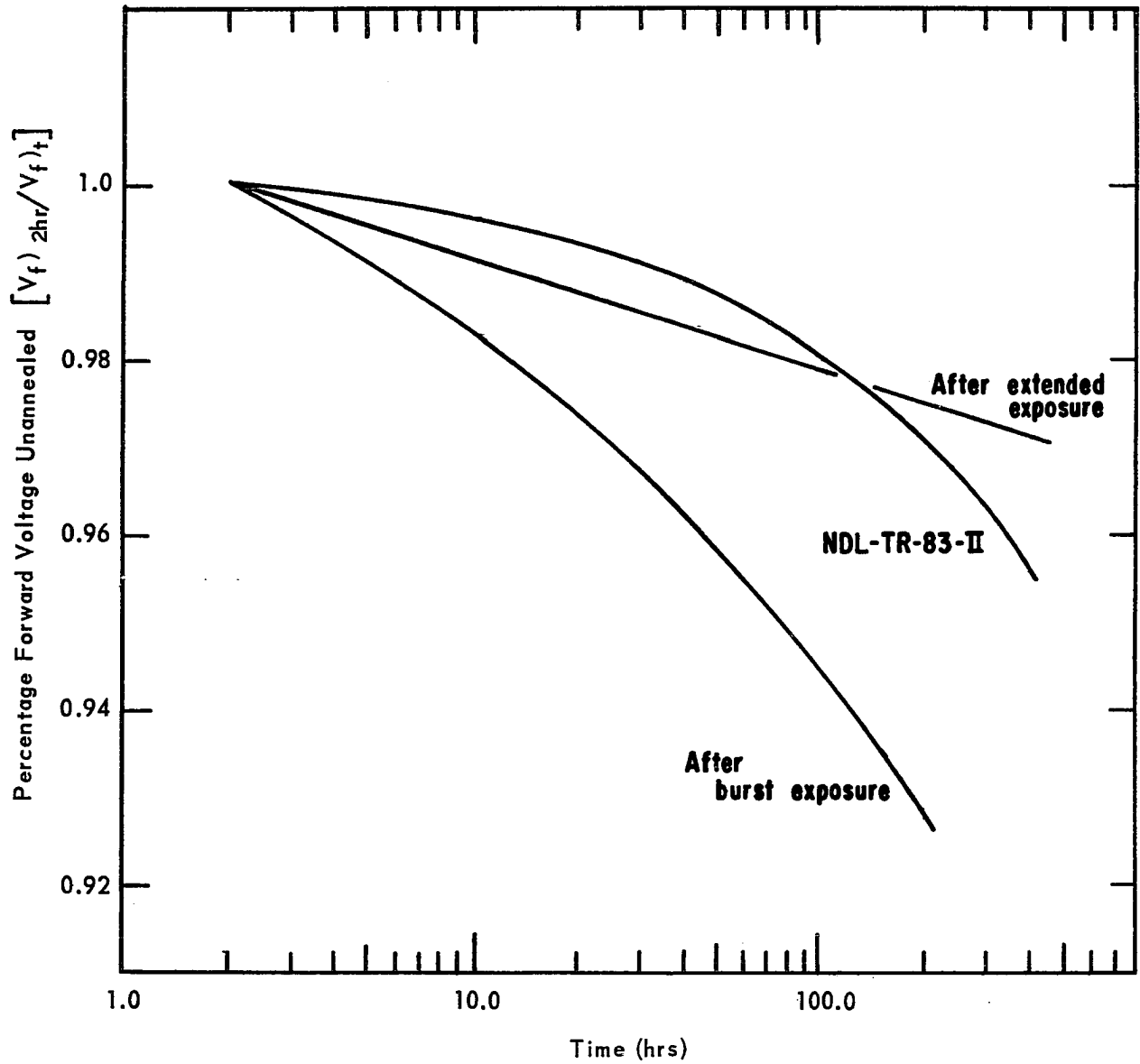


FIG. 8 ROOM TEMPERATURE ISOTHERMAL ANNEAL OF VOLTAGE FOR PH-50 NEUTRON DOSIMETERS

of the extrapolated  $V_f$  at two hours and the  $V_f$  at time  $t$  from exposure stop. The diode recovery from the radiation damage seems to follow an exponential rate for an extended exposure; however, the annealing rate following a burst exposure, except for a greater rate, is quite similar to that reported in the literature.<sup>30</sup>

The dose on each diode was determined by applying the appropriate voltage correction for annealing at the time of read-out to the two hour voltage; the calibration curve supplied the corresponding dose value in rads for the initial and two hour voltage; by subtracting the two dose values, the proper dose to the diode was obtained.<sup>26</sup> Applying this procedure to the HPRR exposure, the average calculated dose was 185.7 rads  $\pm$  13.7% for the twenty-seven diodes exposed at 2.0 m and was 82.6 rads  $\pm$  13.8% for the fourteen diodes exposed at 3.0 m. The errors are stated at the 95% confidence level.

It was noticed that the calculated dose value increased with increasing  $V_f)_i$ . The diode response curve was based on measurements with diodes having a  $V_f)_i \approx 1.00$  volts, but the diodes used in this calibration had  $V_f)_i$  ranging from 0.900 volts to 1.430 volts. Since the sensitivity of the semiconductor device increases with increasing  $V_f$ , it would seem reasonable to expect such a trend in the calculated doses. Consequently, a re-use factor (R), defined as the ratio of the actual dose in rads and the dose based on  $V_f)_2$  hr in

rads, was implemented to correct for this effect. A plot of  $V_f)_i$  versus  $R$ , shown in Figure 9, was plotted from forty data values and was analyzed by linear least squares. The line has a 98.1% correlation with a 2.5% standard error of estimate; its equation is

$$V_f)_i + 1.03 R - 2.07 = 0$$

This correction allows the use of diodes having a wider range of  $V_f)_i$  than formerly possible. Using the calibration results, a dose to the diodes is calculated from the  $V_f$  according to the absolute response curve, corrected for anneal following exposure stop, and corrected for a high initial  $V_f$  with the re-use factor.

As a test for the calibration, twenty diodes were exposed to an unmoderated, fast neutron, burst exposure from the HPRR during the Fourth Nuclear Accident Dosimetry Intercalibration Study on December 6, 1967. The average dose value determined by the eight participants was 479 rads  $\pm$  16.2%. Considering the diodes  $V_f = 1.00$  volt and applying no re-use correction, the calculated average dose was 554 rads, which is a 15.6% relative error. Applying all the corrections, the value was 538 rads  $\pm$  7.8%; this relative error is only 12.3%.

The diode anneal of neutron damage was followed for this group of 46 diodes for 150 hrs after exposure stop. The lower curve on Figure 8 shows an annealing rate with the same relative shape as found in the literature, but with a slightly increased rate.

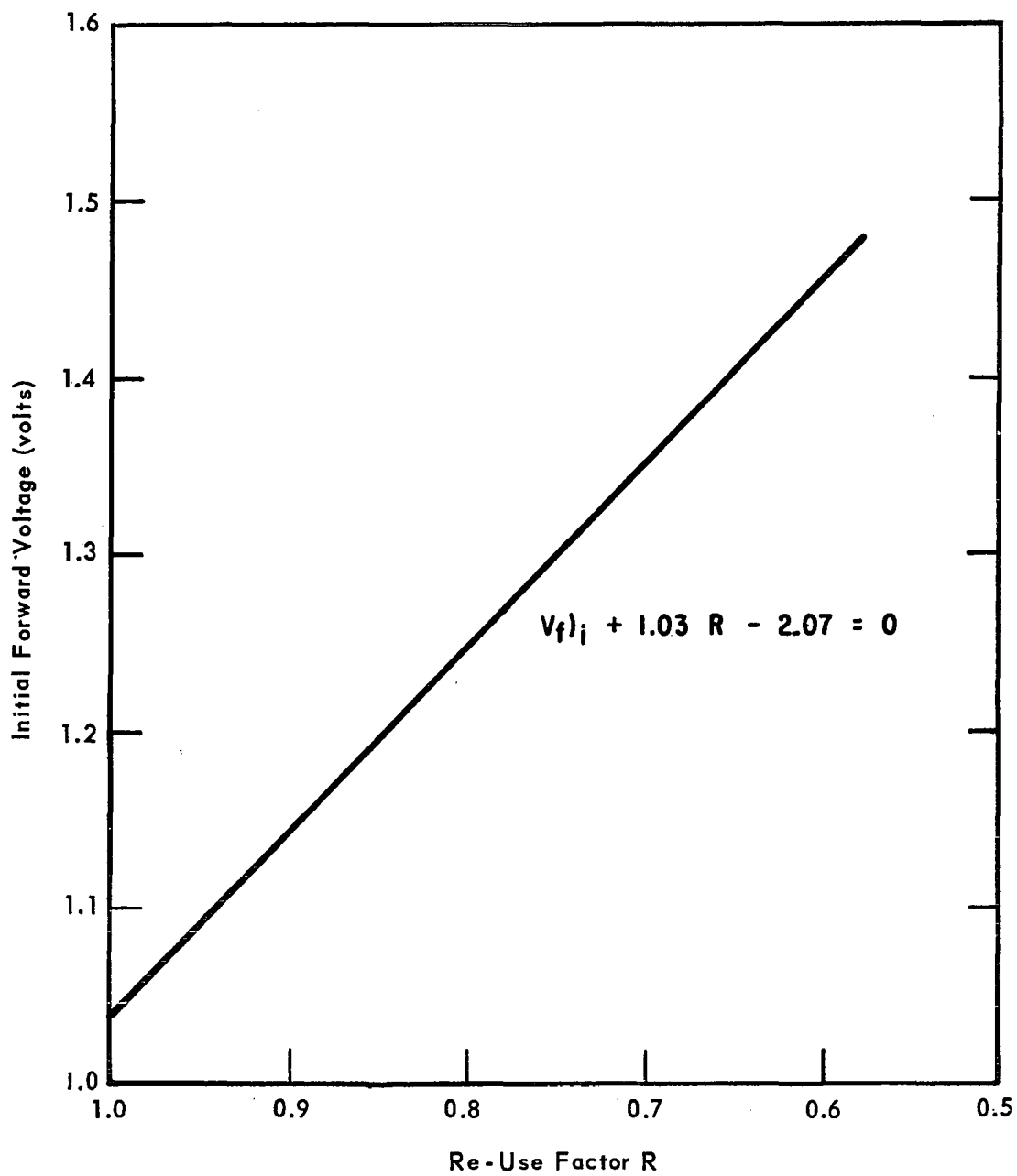


FIG. 9 RELATION BETWEEN INITIAL FORWARD VOLTAGE OF PH-50 NEUTRON DOSIMETERS AND THE RE-USE FACTOR

## CHAPTER IV

### DOSE DISTRIBUTION AROUND A CALIFORNIUM-252 NEEDLE

#### Results

##### Central Axis Depth Dose

The first objective was to determine by two methods the dose rate distribution along a line perpendicular to the central axis of the californium needle at its center. With the source submerged in a phantom filled with T-E solution, this distribution describes the dose rate decrease with increasing thickness of a homogeneous tissue-like material. A plot of the distribution for each of the three activation threshold materials used is shown in Figure 10. At least four measurements were made at each distance for each foil, while as many as eight runs were made for some indium foils.

Similar measurements were performed using the PH-50 fast neutron dosimeters. Five or more determinations were averaged at each point. A plot of the diode results along with the total foil results is shown in Figure 11. The error bars represent the  $2\sigma$  r.m.s. deviation of the diode measurements only. It is seen that both curves show a continuous drop in dose rate reaching about 2.0% of the 0.5 cm dose rate at 4.5 cm depth. The average of deviations for all

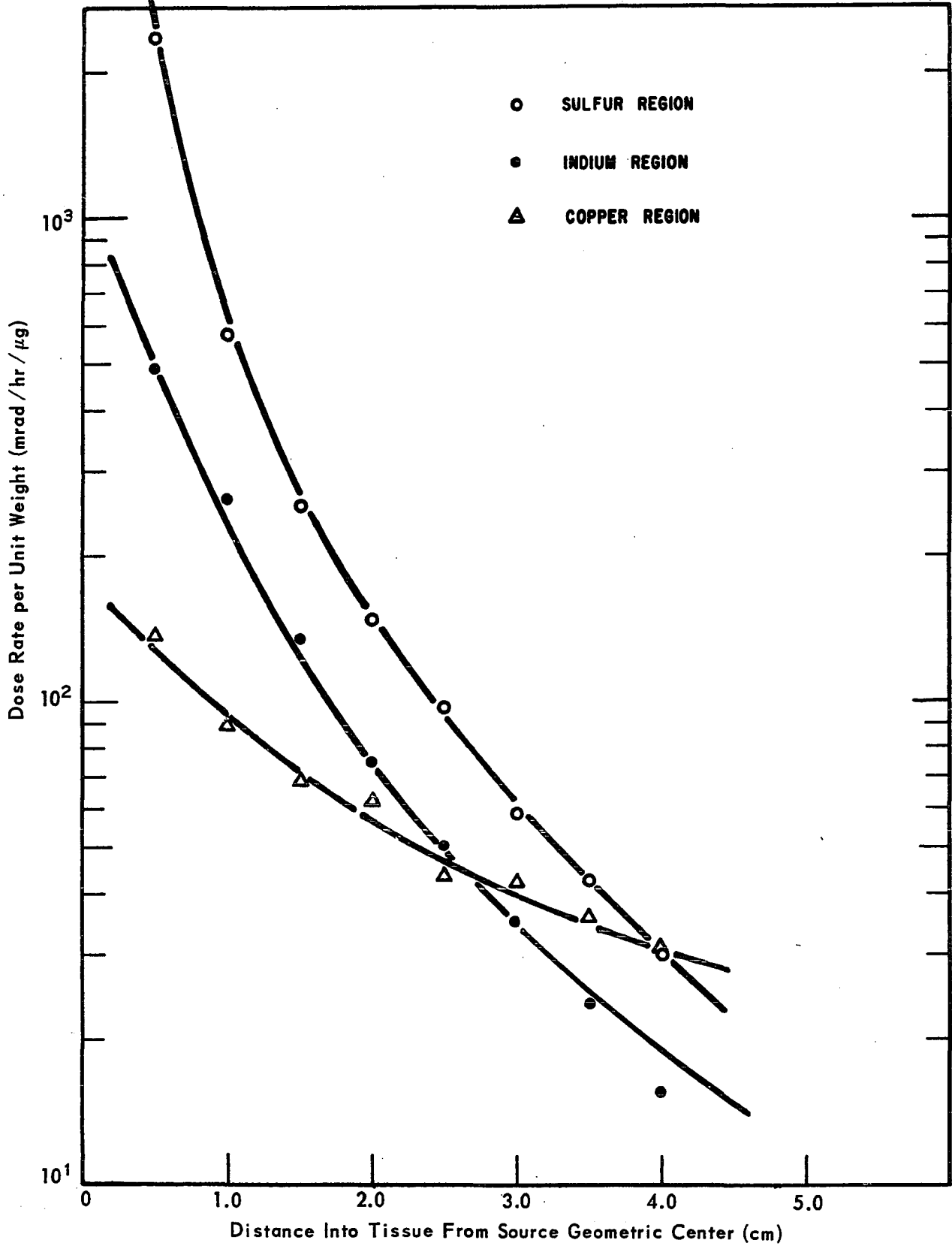


FIG. 10 FOIL MEASURED ENERGY ABSORPTION PER  $\mu\text{g}$  OF  $^{252}\text{Cf}$  AS A FUNCTION OF TISSUE DEPTH

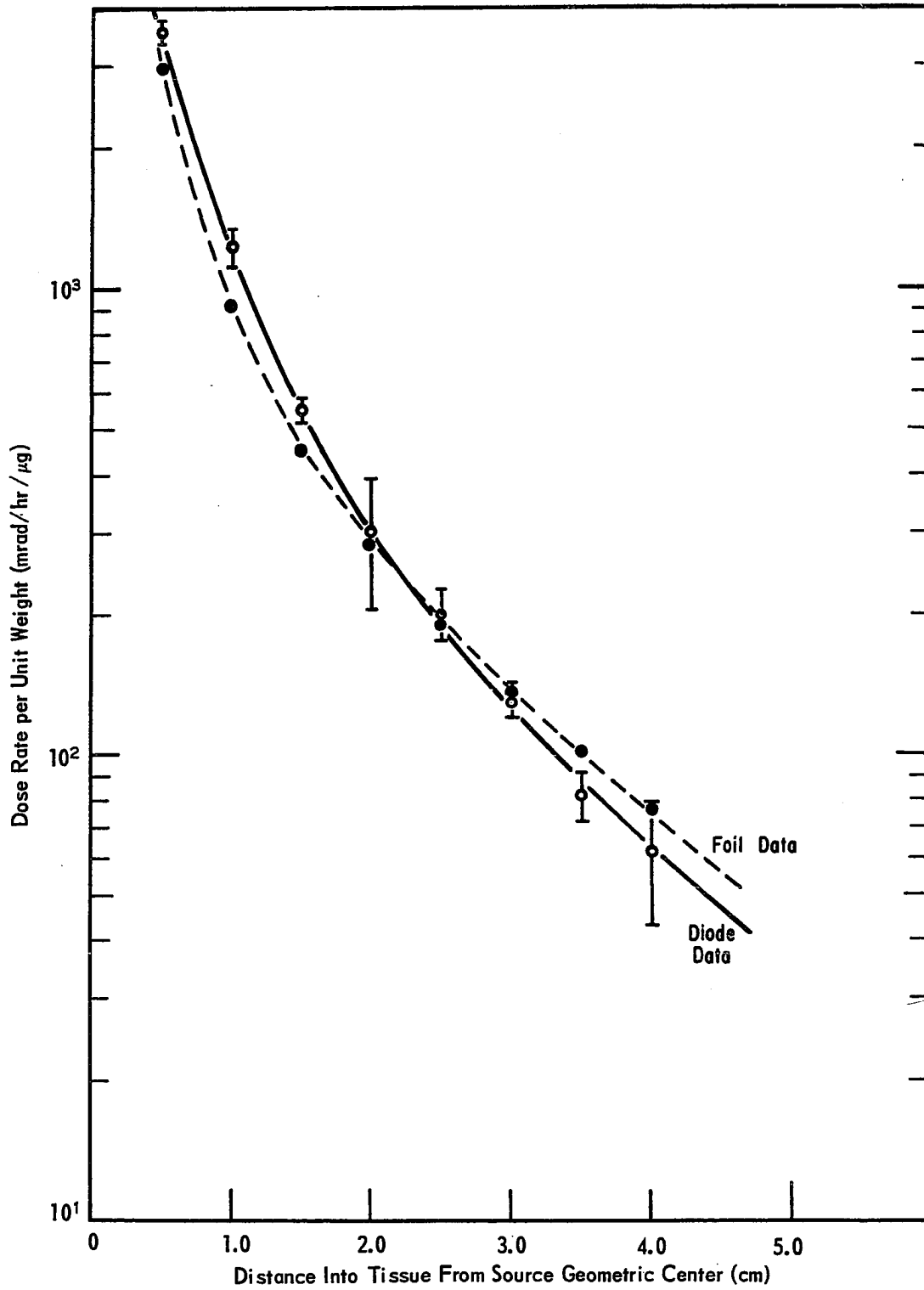


FIG. 11 COMPARISON OF ENERGY ABSORPTION AS A FUNCTION OF TISSUE DEPTH ALONG THE CENTRAL AXIS OF A  $^{252}\text{Cf}$  SOURCE

points was  $\pm 15.7\%$  for the diode method and was  $\pm 55.0\%$  for the foil system. A comparison of the average data and its deviations for both methods is presented in Table 4. The last column shows the percentage difference of the totals at each point.

### Isodose Chart

The other objective was to determine the dose rate distribution over an  $18 \text{ cm}^2$  area lying in the same plane as the needle. Since the reliability of the semiconductor dosimeter was established for simulated "in vivo" dose evaluations with the preceding results, this system was used exclusively to define the dose rate at 78 points in a  $0.5 \text{ cm}$  grid over the area. Again a minimum of four measurements were averaged at each point; the data values are shown in Figure 12. Standard deviations ranged from  $3.0\%$  to  $37.0\%$  with the total average deviation being  $18.7\%$  (see Figure 13). Using the information from the longitudinal dose distribution curves shown in Figure 14, the pattern of absorbed radiation energy in the tissue adjacent to the needle can be depicted graphically in the form of an isodose chart as in Figure 15.

### Analysis and Discussion

#### Central Axis Depth Dose

Determination of the radiation intensity at various points around a source requires an equation expressing the

TABLE 4

Central Axis Depth Dose and Percentage r m s Standard Deviation for Two Dosimetry Techniques

Tissue Depth (cms)	Activation Threshold System (mrads/hr/μg)				Silicon Diode System (mrads/hr/μg)	Percentage Difference of Totals
	Copper (0.1-1.0 MeV)	Indium (1.0-2.5 MeV)	Sulfur (2.5->8.0 MeV)	Total (0.1->8.0 MeV)	Total (0.1->8.0 MeV)	
0.5	139. ± 25.%	492. ± 24.%	2350. ± 40.%	2980. ± 40.%	3587. ± 5.7%	18.5
1.0	89.1 ± 35.	263. ± 38.	573. ± 11.	925. ± 53.	1228. ± 9.9	28.1
1.5	69.3 ± 39.	133. ± 53.	254. ± 14.	456. ± 67.	549. ± 5.9	18.6
2.0	63.3 ± 37.	75.8 ± 37.	148. ± 18.	287. ± 55.	298. ± 32.4	3.6
2.5	43.8 ± 13.	49.9 ± 51.	96.7 ± 14.	190. ± 54.	200. ± 11.9	4.9
3.0	42.3 ± 20.	34.8 ± 49.	58.2 ± 20.	135. ± 53.	130. ± 16.8	4.1
3.5	35.7 ± 29.	23.8 ± 49.	42.1 ± 21.	102. ± 60.	81.2 ± 12.8	22.3
4.0	31.9 ± 18.	15.6 ± 54.	30.0 ± 13.	77.5 ± 58.	60.8 ± 30.0	24.1
	<u>Avg. ± 27.%</u>	<u>Avg. ± 44.%</u>	<u>Avg. ± 16.%</u>	<u>Avg. ± 55.%</u>	<u>Avg. ± 15.7%</u>	

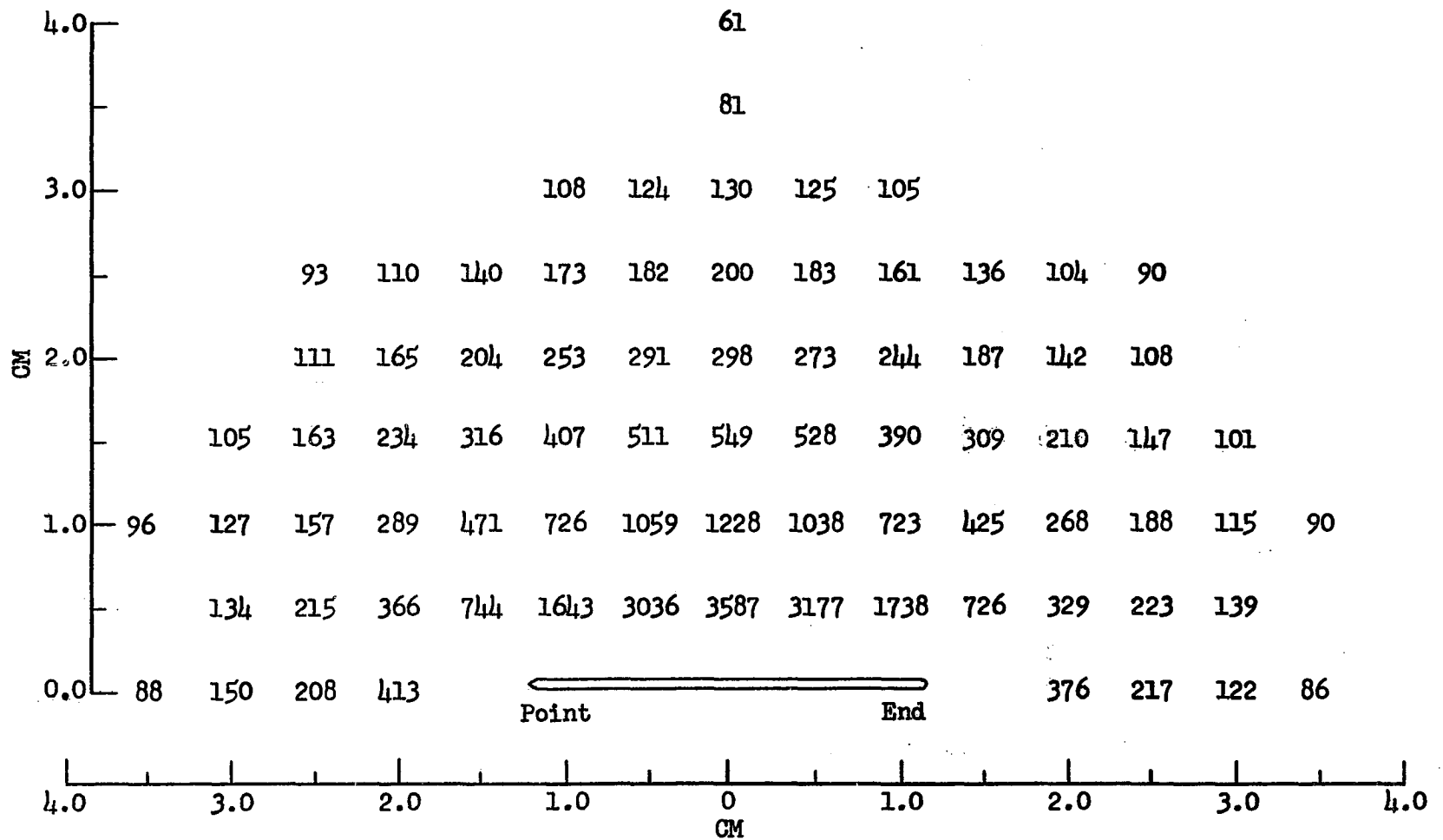


FIG. 12 FAST NEUTRON DOSE DISTRIBUTION AROUND A <sup>252</sup>Cf NEEDLE  
 (The units are millirad/hr/μg of Cf.)

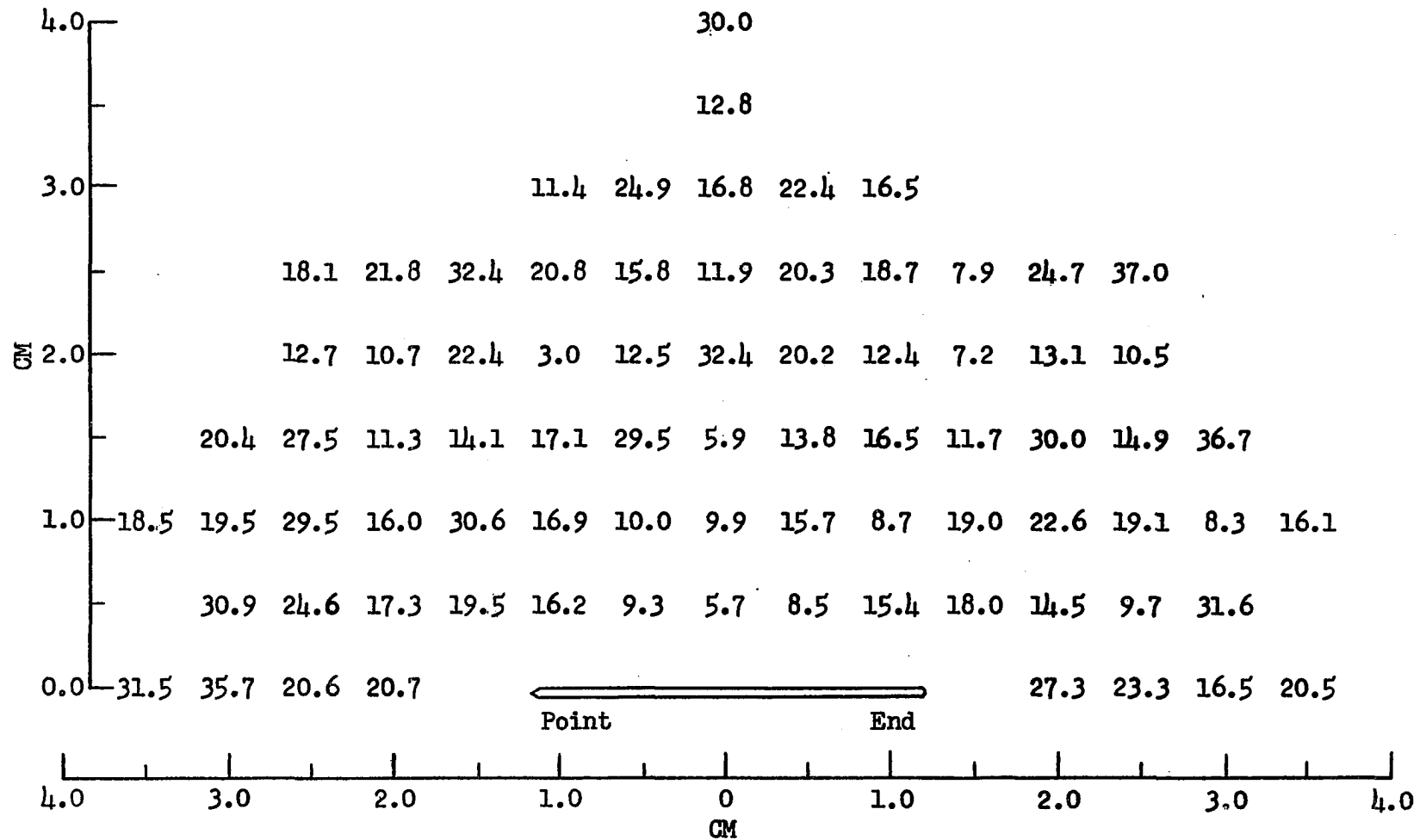


FIG. 13 DISTRIBUTION OF THE PERCENTAGE DEVIATION FROM THE AVERAGE FOR THE FAST NEUTRON DOSE AROUND A  $^{252}\text{Cf}$  NEEDLE

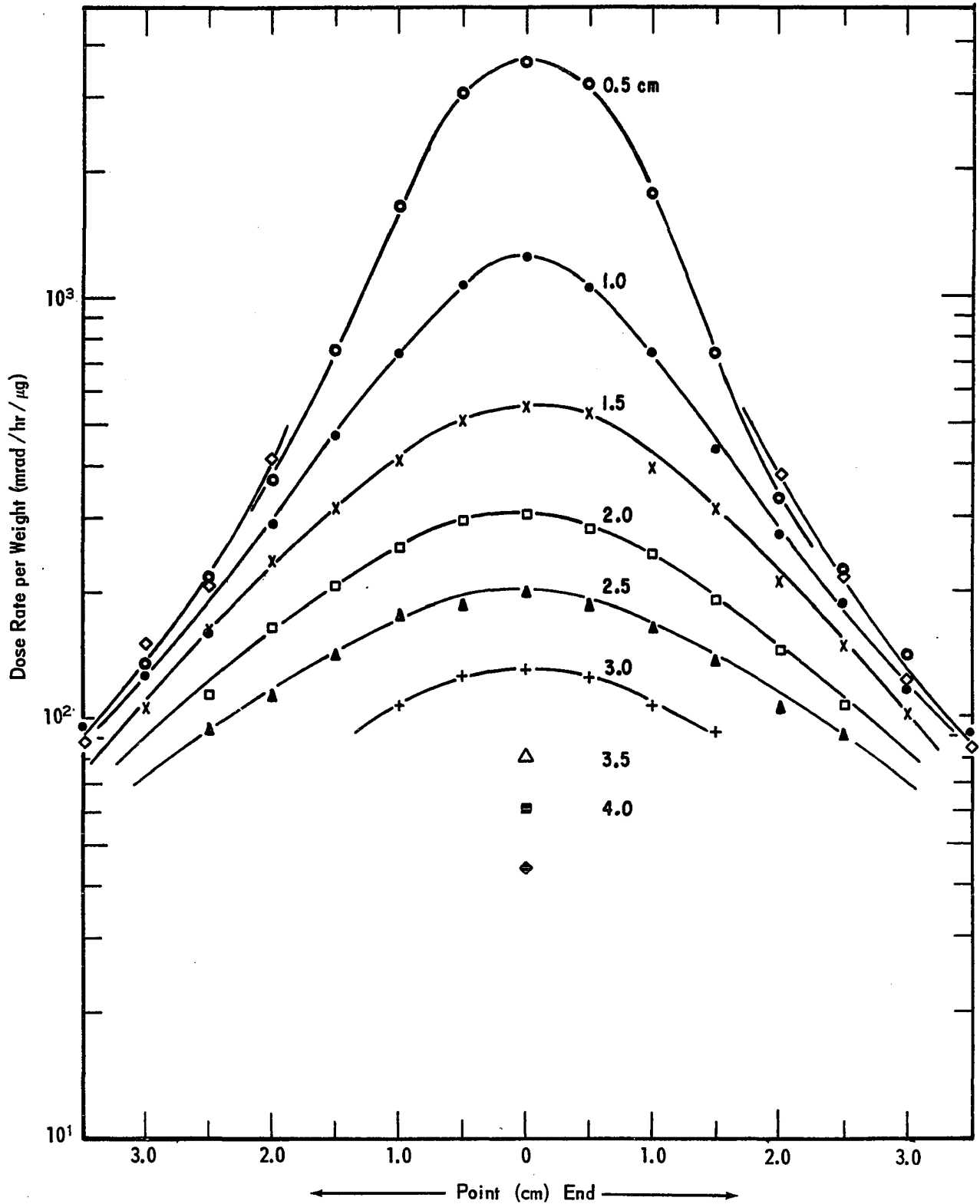


FIG. 14 LONGITUDINAL DISTRIBUTION OF DOSE FROM A  $^{252}\text{Cf}$  NEEDLE  
(Diode Measurements)

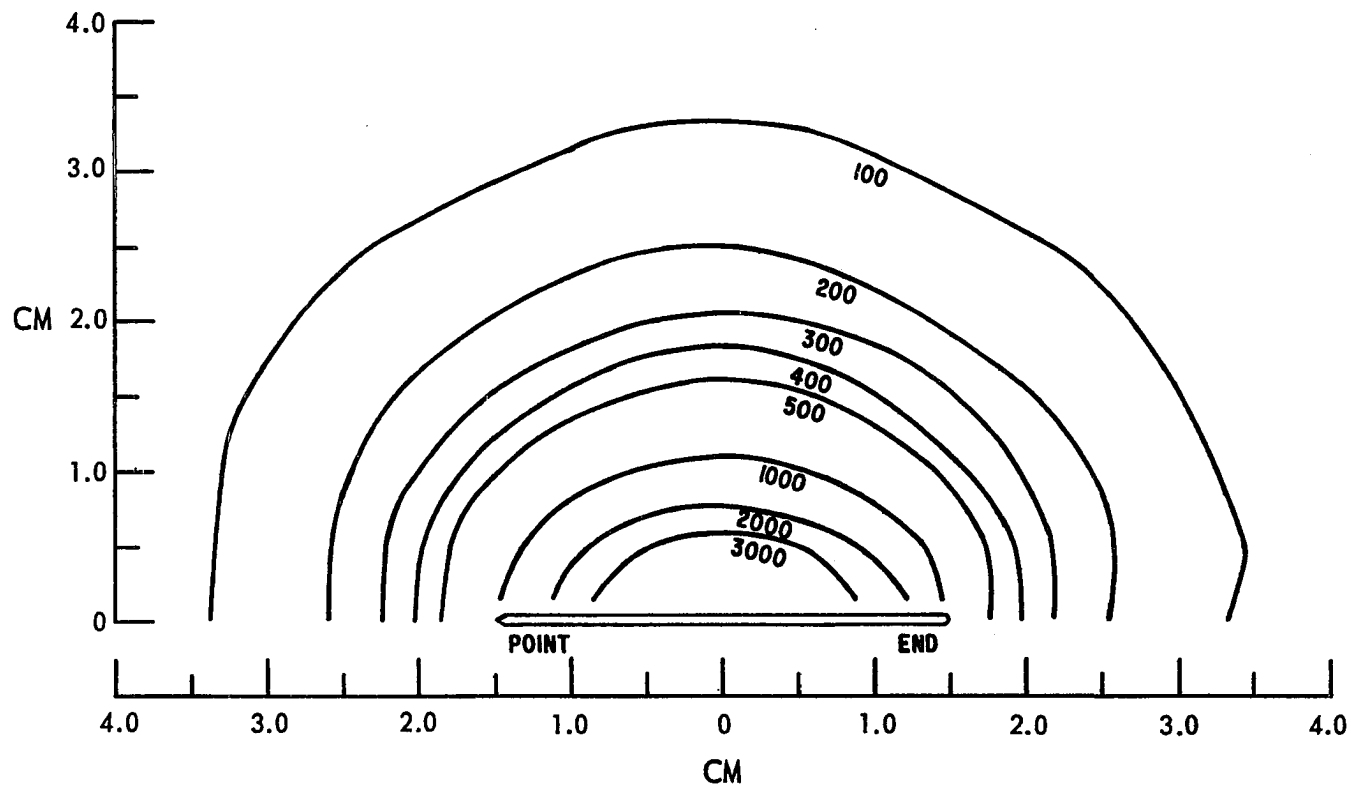


FIG. 15 FAST NEUTRON ISODOSE CHART FOR A  $^{252}\text{Cf}$  NEEDLE  
(The units are in millirads/hr/ $\mu\text{g}$  of Cf.)

geometric relations between the source and the detector. The experimental arrangement of exposure for the central axis dose data of Figure 11 is shown in Figure 16.

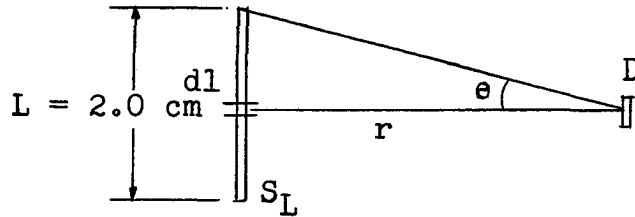


FIG. 16 GEOMETRY OF EXPOSURE FOR THE LINE SOURCE AND DETECTOR.

The contribution of  $dl$  to the flux ( $\phi_D$ ) can be summed over  $L$  to determine the radiation flux at point  $D$  by using the expression of Sievert's Integral:

$$\phi_D = \frac{BS_L}{2\pi r^2} \int_0^\theta e^{-\mu r \sec \theta} d\theta$$

$S_L$  is the source strength,  $B$  is the buildup factor, and  $\mu$  is the absorption coefficient.<sup>50</sup> The integral in the expression lends itself to evaluation by the approximation method of Gaussian numerical integration.<sup>51</sup> Once the flux at a point is known, only the neutron energy spectrum is needed in order to calculate the neutron dose.

The data for central axis depth dose can be fitted to a simpler exponential form:

$$D_x = (D_{0.5} B e^{-X/L})(1/X).$$

$D_x$  represents the neutron dose rate under the conditions established by any particular value of tissue thickness  $x$ ;

$D_{0.5}$  is the dose rate at 0.5 cm from the source center along the central axis in tissue-equivalent (T-E) solution;  $B$  is the buildup factor due to the presence of material in the radiation field; and  $L$  is the relaxation length. This exponential fit is justified as an empirical fit only; no theoretical significance is attached to it. An exponential fit, based on diode measurements, is shown in Figure 17 with relation to a  $1/x$ ,  $1/x^2$ , and  $1/x^3$  dependence. The line for  $f(x) = x$  represents the data with the inverse distance factor removed. Thus, the resulting straight line shows only the dose dependence on the intervening tissue thickness. When analyzed by linear least squares method, the data has a 99.3% correlation to the exponential fit. The similar data for the foil measurements has a 98.3% correlation. Mathematically, it was expedient to minimize the logarithm function rather than the equation, i.e.

$$\sum_i [\{\ln(B) - X_i/L\} - \ln(X_i D_x/D_{0.5})] = \text{minimum}$$

From this minimization, the two constants characteristic of the source and the phantom are  $L = 2.73$  cm for relaxation length and  $B = 0.216$  for buildup factor. It can not be assumed that the neutrons were striking normally or uniformly on the detector volume. This value for  $L$  would be increased slightly if a point source was used. The value of  $L$ , as well as  $B$ , is dependent on the phantom size, especially when the phantom is small.<sup>52</sup> It should be noted that  $L$  has approximately the same value with increasing tissue thickness when

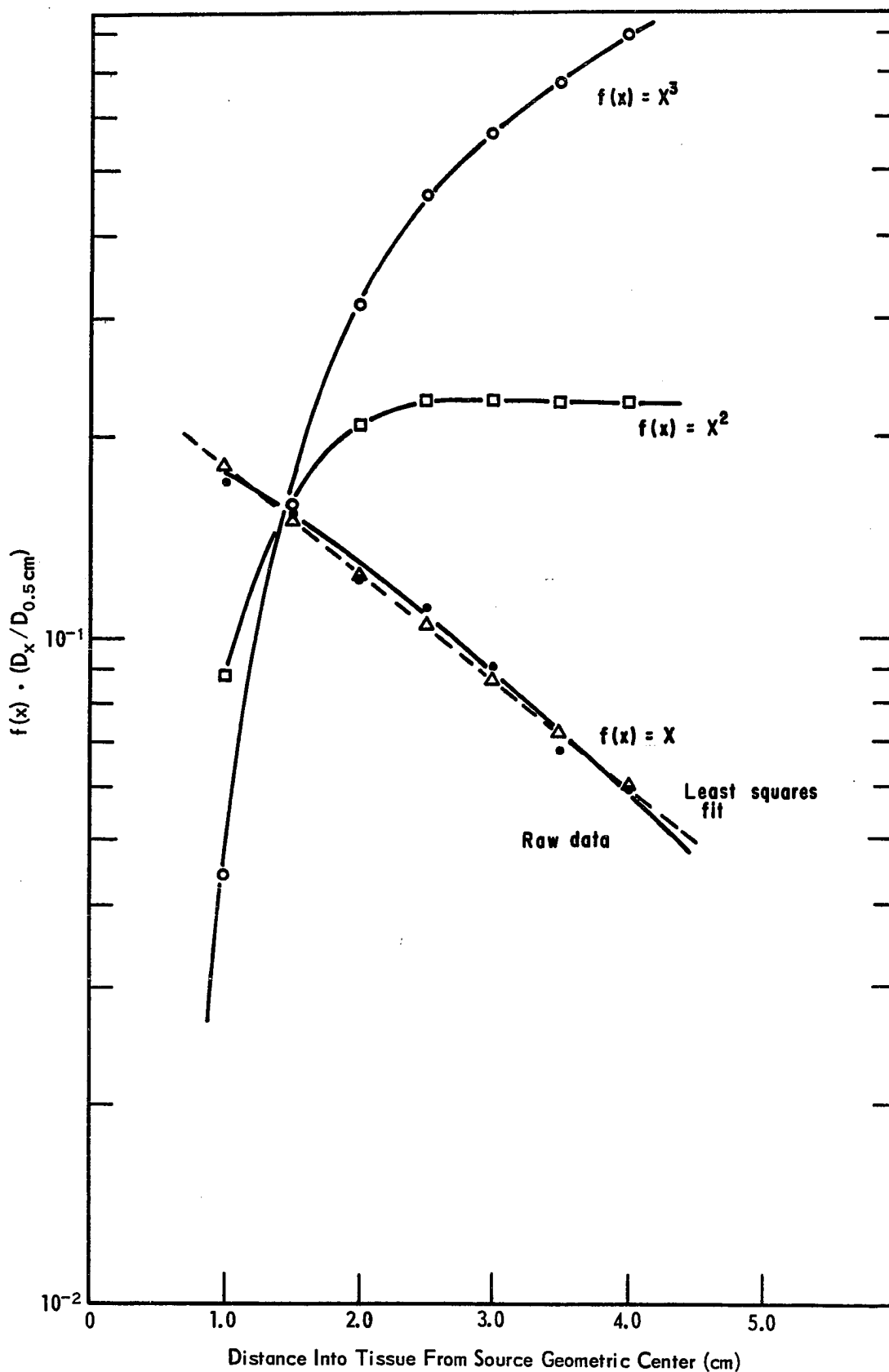


FIG. 17 EXPONENTIAL FITS OF DEPTH DOSE DATA AS A FUNCTION OF TISSUE DEPTH SHOWING THE DEPTH DEPENDENCE

measured in terms of dose, if the neutron energy spectrum does not change significantly with depth in tissue.

Deviation of the diode data from a true exponential relationship may be due to this spectral alteration. When the percentage dose in each energy interval covered by the three activation foil materials is plotted as a function tissue thickness, a spectral change is apparent. A beam of neutrons with mixed energies traversing a T-E phantom may experience two processes, namely filtration of the lower energy components and degradation of all parts of the spectrum by scattering. These processes act in opposite directions in producing spectral shifts with depth. Filtration would not be evident in these dose considerations since low energy neutrons contribute only a small fraction of the total fast dose. Scattering causes a reduction in mean energy at a depth and is the reason for depth dose decrease.

Field and Parnell studied the changes in a fast neutron spectrum with increasing depth in a T-E phantom, using activation threshold materials.<sup>53</sup> They concluded that filtration was the reason for a slight upward shift of the spectrum with depth. The lowest limit of the energy range considered was 2.9 MeV; consequently, their observations do not pertain to the total effect on redistribution of the fast neutron dose. When the consideration is expanded to include neutron energies down to 10 keV, the spectral change, and corresponding dose redistribution, is evidently due to degradation. As seen

from Figure 18, the dose percentage in the copper region builds up at the expense of the indium and sulfur regions, mostly the sulfur region. At some distance greater than 4.0 cm the dose in the copper region would reach a maximum, then decrease rapidly. Such changes in spectral shape are important to consider for a therapeutic application because the RBE and oxygen enhancement ratio of the radiation field at a depth might be altered in relation to their values at the surface.

The two methods for dose distribution measurement show good agreement. Certainly, the PH-50 diode system exhibits greater precision and convenience than the foil system. The relative error between systems ranges from 3.6% at 2.0 cm to 28% at 1.0 cm. One system can not be preferred for the other with respect to accuracy. No particular significance is attached to the crossing of the curves in Figure 11; however, it can be explained. The diodes have an energy dependence that drops off quite rapidly below 0.3 MeV. Degradation of the neutron energies must have become significant enough at depths  $>2.0$  cm to correspond with the slight decrease in diode sensitivity. Foil measurements at such depths would achieve greater accuracy by approaching ideal point detector-source conditions. On the other hand, diode measurements close to the needle, ( $<2.0$  cm ) have optimum sensitivity and better geometry conditions for exposure than the foils.

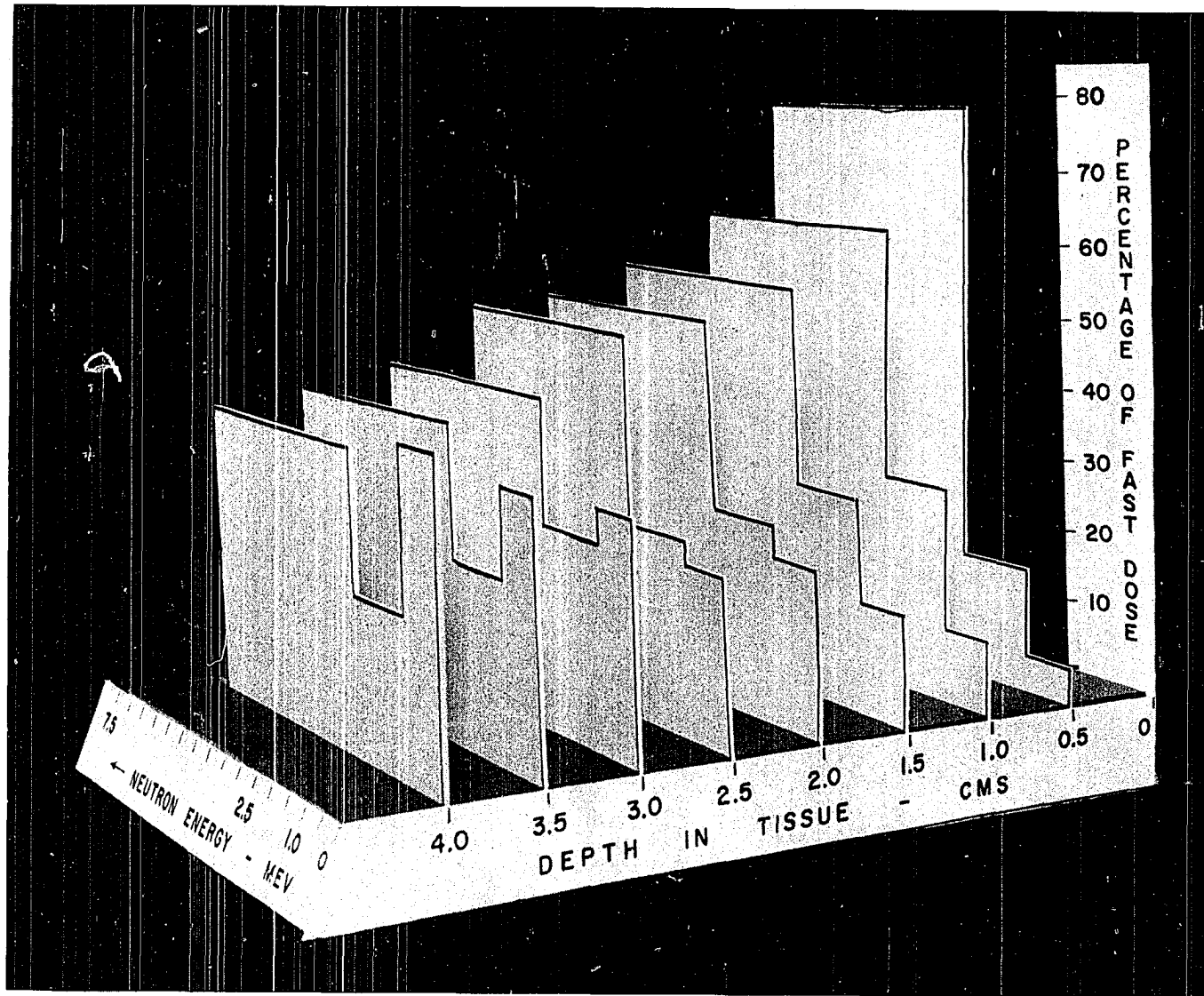


FIG. 18 RELATIVE NEUTRON DOSE PERCENTAGE CHANGE AS A FUNCTION OF TISSUE DEPTH WITH NEUTRON ENERGY AS THE PARAMETER

A point to consider when referring to accuracy of the diode measurements is that the HPRR spectrum, used for calibration, is a softer spectrum than that of  $^{252}\text{Cf}$ , as shown in Table 2. Although the energy dependence and sensitivity of the diode vary as the one-third power of the neutron energy, the changes in the neutron energy distribution of the californium spectrum with increasing moderation and of the HPRR fission spectrum in the narrow range of 0.1-8.0 MeV have been assumed to introduce negligible differences in evaluations of the fast neutron dose.

The largest error of the diode technique lies in the inaccuracy for rate of room temperature isothermal annealing processes during and after exposures, especially extended exposures. An analysis of these processes, first reported by Chase et. al.<sup>27</sup>, showed rates, based on voltage anneal, as much as 30% less than that reported by Swartz et. al.<sup>28</sup>. The analysis of a large population of diodes (41) reported herein (Figure 8) shows an average difference of 2.6% in voltage regeneration after exposure to a burst or to an extended exposure. Although the observed difference is small for voltage consideration, projected to dose calculations, the error due to inaccurate annealing corrections could be as high as 35% depending on the dose and  $V_f)_i$  of the diode. The dosimeters are dose rate independent, but they are time dependent. So, some type of anneal takes place during long runs such as those required for this investigation. If an

exponential rate of anneal is assumed, the exposure annealing which occurs for runs within sixty hours time has no appreciable effect on the final  $V_f$ ; therefore, all anneal corrections were made from the time of exposure stop.

Another source of error is associated with the actual read-out of the diode. Care was exercised to prevent heat buildup ( $i^2R$ ) from the inherent diode resistance. For some voltages, especially large  $V_f$  values (1.8 volts), the temperature change associated with sustained read-out caused as much as 100% error. When the voltage rise due to neutron bombardment is very large, as much as 15 volts, pulsed read-out techniques are required.<sup>54</sup>

Although the diodes are temperature dependent, the small variation from room temperature ( $\pm 3^\circ\text{F}$ ) during storage and exposure has an inconsequential effect on the precision of the dosimeters. An error of  $\pm 0.025$  volts persists in read-out regardless of the  $V_f$ . Error due to graphical interpretation of the calibration curve amounts to about  $\pm 2$  rads for any  $V_f$ . Ultimately, the complete analysis indicated and the good correlation with the expected result established that the semiconductor PH-50 neutron dosimeters are a convenient, dependable, and precise technique for measuring fast neutron dose in a T-E material.

In regard to the foil system, the agreement with the expected results is acceptable. The copper, indium, and sulfur measurements have average errors at the 95% confidence

level of  $\pm 27\%$ ,  $\pm 44\%$ , and  $\pm 16\%$ , respectively. These errors compare favorably with the diode system error. The total average deviation, which reflects a compound error from the three foils, is  $\pm 55\%$ .

Further analysis indicates a large error is contributed by the indium foil measurements. Detection of the foil activation by a scintillation technique at a low-level foil activity is difficult because of the high background. The method of calculation involves subtracting two count rates near background level. This method is necessary because a slightly higher energy gamma ray contributes an interfering Compton electron distribution. Another error, ordinarily insignificant, is the shift in analyzer gain, which affects the gross counts under the desired photopeak. It was determined that the error of dose measurement with the indium foil increased with tissue thickness due to the relative change in contribution to activation from the interfering  $(n,\gamma)$  reaction; as the spectrum was degraded by increasing moderation, the  $^{116m}\text{In}$  activation increased. A compounded error is present in the dose values computed from the intermediate flux because this flux is the difference between the indium and sulfur measured fluxes and combines the errors from each measurement.

#### Isodose Chart

Since the results from the two dose measurement techniques show good agreement for the depth dose data, the PH-50

diode method was the logical choice for use in establishing the neutron isodose curves around the californium needle. All the previous comments concerning error in the diode technique apply here too. An average deviation for all points at the 95% confidence level is 18.7%. This is an increase from the over-all average error of the depth dose data. At least five measurements were made at each point and averaged for the data in Figure 15.

The precision of measurement decreases with increasing distance from the source because of the low dose rates. Long exposure times (up to 60 hrs) were required to achieve a detectable change in the diode electrical characteristics. The reported values for dose rate at distances from the needle are slightly low as previously indicated by the central axis depth dose curve. The error is present because of the slight drop in diode sensitivity accompanying each degrading change in the neutron energy spectrum.

The longitudinal distribution of dose rate shows a slight skewness away from the eyelet end of the needle. The reason for this is that the neutron flux at the eyelet end is depressed, possibly due to the attenuation achieved in the threaded cap, which has about 30% more platinum than has the point. Since the curves tend to converge with increasing distance from the needle center and since the peaks flatten, it appears that isodose contours approach a circle. The isodose chart of Figure 15 is derived from interpolation of the longitudinal and of the radial plots of the distribution data.

## Chapter V

### CONCLUSIONS

Silicon diode dosimeters and activation threshold foils were two methods useful to measure the dose distribution around a linear  $^{252}\text{Cf}$  source. The semiconductor device (PH-50) relates its change in forward voltage to the fast neutron dose incident from a fission spectrum. Dose values had accuracy to within  $\pm 10\%$  and had precision of  $\pm 7\%$  for doses  $>25$  rads. The foil system relates the material induced activity to the neutron dose above 0.1 MeV. The foil dose values had less accuracy (20-30%) depending on the accuracy of cross section values. Since the activation and the methods of counting induced activity depend on statistical processes and since compounded errors arise from the method of dose calculation, the foil technique had low precision ( $\pm 50\%$ ).

Comparison of the depth dose data from each method shows good agreement, however. The two curves have less than 28% relative error for all points. The neutron dose per  $\mu\text{g}$  of  $^{252}\text{Cf}$  drops about 100-fold in the region from 0.5 cm to 4.5 cm. In comparison the  $\gamma$ -ray dose per mg of radium drops 100-fold from 0.5 cm to about 8.0 cm. It is apparent that localization of dose in tissue is greater with neutrons from one  $\mu\text{g}$

of Cf than with  $\gamma$ -rays from one mg of radium.

The silicon dosimeters were used to establish the distribution of dose on a plane around the neutron source. An isodose chart shows that only a slight distortion of the dose occurs near the ends of the needle. The isodose contours approach a circle at distances greater than 4.0 cm. Evidently, a small radioactive neutron source of  $^{252}\text{Cf}$  has advantages over conventional methods for radiotherapy applications.

Microgram quantities of  $^{252}\text{Cf}$  allow versatility of treatment with high LET neutrons in a form never before available. Considering dose distribution, quality of radiation, availability, and economy,  $^{252}\text{Cf}$  is a good substitute for radium and other implantable  $\gamma$ -ray sources.

The work presented here is only one of the few basic steps required to gain knowledge for medical applications of neutrons. The OER of an implanted n- $\gamma$  source, which could vary from the OER of a beam n- $\gamma$  source, must be investigated. The effect of an implanted neutron source on the LET distribution as a function of tissue thickness must be considered. Knowledge of the acute and protracted RBE for the mixed radiation of  $^{252}\text{Cf}$  will be necessary before use is advised. The physical dose aspects of  $^{252}\text{Cf}$   $\gamma$ -rays are now being investigated. Regardless of how complete laboratory investigations of Cf are, the cancer problem will not be solved until it is brought back to the patient in the clinic.

## APPENDIX A

### EVALUATION OF WEIGHTED AVERAGE KERMA/FLUENCE FACTOR

The coefficients in the equation on page 19 represent averaged factors, weighted for the  $^{252}\text{Cf}$  neutron spectrum, which convert the neutron fluence to an equivalent neutron dose in rads. The following equation defines the dose conversion factor:

$$\bar{C}(E) = \frac{\int_0^{\infty} \phi(E) C(E) dE}{\int_{E_1}^{E_2} \phi(E) dE}$$

where  $\phi(E)$  is the  $^{252}\text{Cf}$  neutron flux per unit energy<sup>44</sup>,  $C(E)$  is the differential KERMA/fluence<sup>20</sup> times 0.01 rad/erg/g, and  $E_1$  and  $E_2$  are the energy boundaries for the factor. For a plane source, flux may be replaced by neutron current:

$$\bar{C}(E) = \frac{\int_0^{\infty} N(E) C(E) dE}{\int_{E_1}^{E_2} N(E) dE}$$

where  $N(E)$  is the number of neutrons per unit energy. Since evaluation of  $\bar{C}(E)$  involves rigorous mathematical treatment, the expedient method is by graphical integration. Figure 19 is a plot of  $C(E)$  and  $N(E)$  versus neutron energy. A particular energy interval was selected first, e.g. 2.5 to 8.0 MeV.

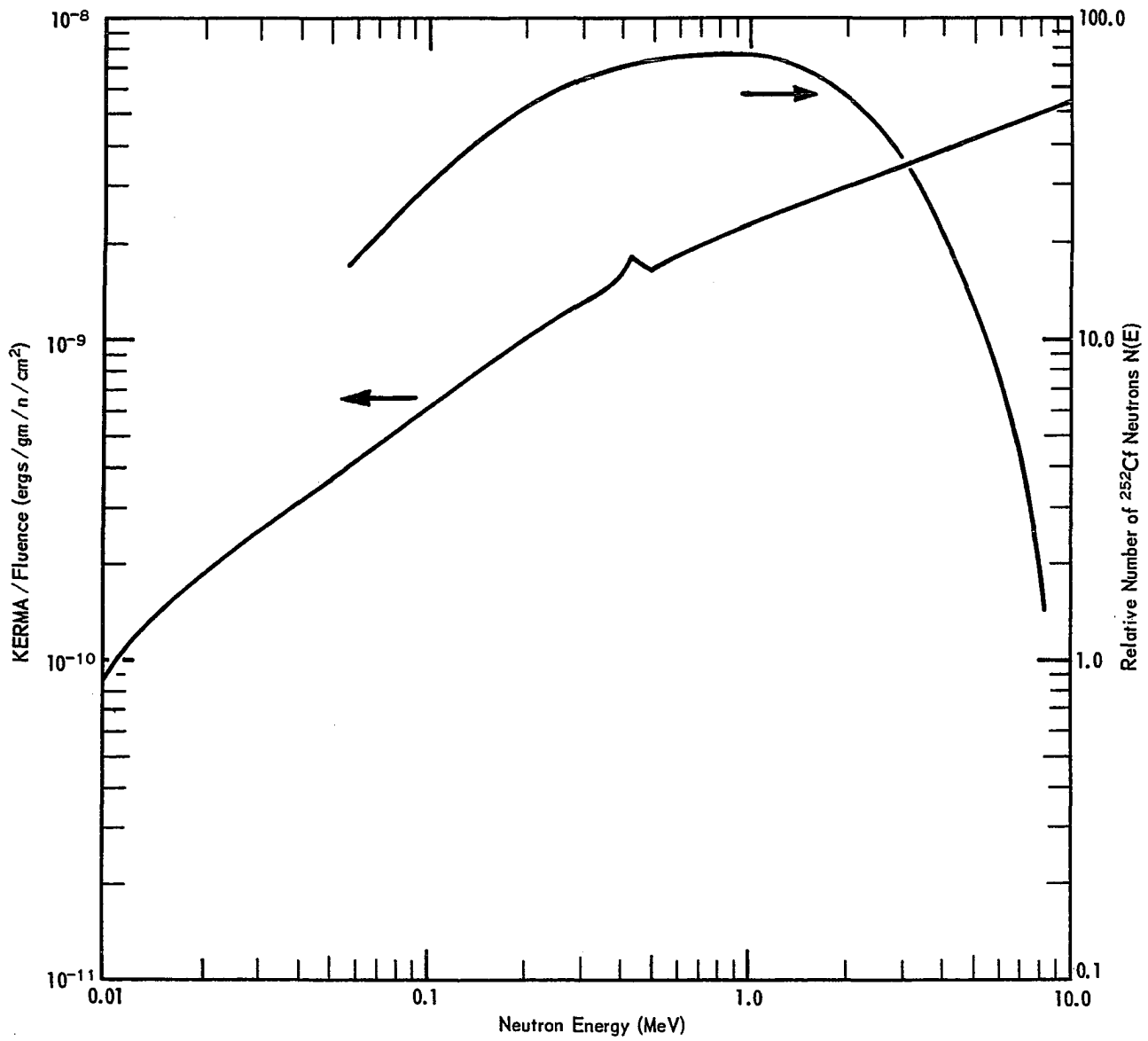


FIG. 19 SIMULTANEOUS PLOT OF KERMA/FLUENCE AND RELATIVE <sup>252</sup>Cf FISSION NEUTRON SPECTRUM AS A FUNCTION OF NEUTRON ENERGY

An energy increment of 0.1 MeV was specified. Then the appropriate  $N(E)$  and  $C(E)$  were determined at the mid-point of each increment, e.g. at 2.5-2.6 MeV  $N(E) = 45.0 \text{ n/cm}^2$  and  $C(E) = 3.24 \times 10^{-9} \text{ rads/n/cm}^2$ . All the incremental  $N(E) \cdot C(E)$  for the energy interval were added and divided by the number of increments in the interval to obtain the weighted average  $C(E)$ . Table 3 presents the values of conversion factors for two neutron spectra.

## APPENDIX B

### CALCULATIONS FOR THE ACTIVATION THRESHOLD SYSTEM

The following calculations present the method used to calculate neutron flux in  $n/cm^2/sec$  from the basic count rate of the activation foil material.

#### Lower Flux (2.0 eV to 1.0 MeV)

As stated in Chapter II-C, the copper foil ( $n, \gamma$ ) activation reaction can be used to relate the induced activity as measured by a GM-type counter to the incident neutron flux. The specific equation and pertinent constants follow:

$$\phi_{Cu} = FCU = \frac{(CPMC)(QC)(CLFC)}{(WC)(K)(N_T)(\sigma_{eff})(1-e^{-\lambda_{TOC}})(e^{-\lambda_{TIC}})(60)} \text{ n/cm}^2/\text{sec},$$

where, FCU = copper measured flux - name used in computer code,

CPMC = copper count rate less background from GM counter,

QC = counter efficiency factor at time of count based on  $^{90}\text{Sr}$ - $^{90}\text{Yt}$  standard = 2.16 d/c (ctr. A) and 2.23 d/c (ctr. B),

CLFC = calibration factor for copper = 1.51 n/d,

WC = weight of two  $7/32$ inD copper foils = 0.0520 g,

K = natural abundance of copper-63 = 0.69,

$\sigma_{\text{eff}}$  = effective cross section for fission spectrum =  
 $0.258 \times 10^{-24} \text{ cm}^2$ ,

$N_T = 9.48 \times 10^{21} \text{ nuclei/g}$ ,

$\lambda = \text{decay constant} = 9.0 \times 10^{-4} \text{ min}^{-1}$ ,

TOC = exposure time in minutes,

TIC = time from exposure stop to mid-time of counting interval in minutes.

The equation simplifies to:

$$\phi_{\text{Cu}} = (14.92) \frac{(\text{CPMC})(\text{QC})}{(\text{WC})(1-e^{-\lambda\text{TOC}})(e^{-\lambda\text{TIC}})} \text{ n/cm}^2/\text{sec.}$$

#### Intermediate Flux (1.0 to 2.5 MeV)

The flux from 1.0 to 8.0 MeV was determined by the induced activity of an indium foil due to the (n,n') reaction. Gamma spectroscopic analysis was required as previously stated. The pulse height analysis system was calibrated to  $^{115\text{m}}\text{In}$  gamma-rays; channels 31-35 inclusive contained the 0.335 MeV peak above the FWHM level. Since the 0.400 MeV peak belonging to the gamma-ray from the (n, $\gamma$ ) reaction is contributing counts to the specified channels, two sample counts must be made. Due to the different half-lives of In-115m and -116m, the relative change of the 0.335 MeV peak for a known decay time between counts can provide an uncontaminated count total due only to the  $^{115\text{m}}\text{In}$  gamma-ray.

Let A = number of counts from  $^{116\text{m}}\text{In}$  (54 min. half-life),

B = number of counts from  $^{115\text{m}}\text{In}$  (270 min. half-life),

t = time elapsed from start of first count to start of second count in minutes.

$$A + B = (\text{1st gross cts. in channels 31-35}) \text{ minus} \\ (\text{background in ch. 31-35}).$$

$$(A)(e^{-0.693t/54}) + (B)(e^{-0.693t/270}) = (\text{2nd gross cts. in} \\ \text{ch. 31-35}) \\ \text{minus (background in ch. 31-35)}.$$

Combining the two equations:

$$B = \frac{\left[ \left( \frac{\text{2nd gross cts. in Ch. 31-35}}{\text{Ch. 31-35}} \right) - \left( \frac{\text{BG in Ch. 31-35}}{\text{Ch. 31-35}} \right) \right] - \left[ \left( \frac{\text{1st gross cts. in Ch. 31-35}}{\text{Ch. 31-35}} \right) - \left( \frac{\text{BG in Ch. 31-35}}{\text{Ch. 31-35}} \right) \right] e^{-\frac{0.693t}{54}}}{e^{-0.693t/270} - e^{-0.693t/54}}$$

Dividing B by the counting interval in minutes gives CPMG, the counts per minute due to the (n,n') reaction. The equation and constants to calculate neutron flux follow:

$$\phi_{\text{In}} = \text{FG} = \frac{(\text{CPMG})(\text{CLFG})}{(\text{WG})(\text{K})(\text{N}_T)(\sigma_{\text{eff}})(1 - e^{-\lambda \text{TOG}})(e^{-\lambda \text{TIG}})(60)} \text{ n/cm}^2/\text{sec},$$

where, FG = indium measured flux above 1.0 MeV - name used in computer code,

CPMG = net indium count rate obtained from B,

CLFG = calibration factor for indium = 1.50 n/c,

WG = weight of two  $7/32$  in D indium foils = 0.0468 g,

K = natural abundance of indium-115 = 0.958,

$N_T = 5.247 \times 10^{21}$  nuclei/g,

$\sigma_{\text{eff}} = 0.155 \times 10^{-24}$  cm<sup>2</sup>,

$\lambda = \text{decay constant} = 2.62 \times 10^{-3}$  min<sup>-1</sup>,

TOG = exposure time in minutes

T1G = time from exposure stop to mid-time of counting interval in minutes.

The equation simplifies to:

$$\phi_{In} = (21.4) \frac{(CPMG)}{(WG)(1-e^{-\lambda T OG})(e^{-\lambda T1G})} \text{ n/cm}^2/\text{sec.}$$

In order to obtain the flux from 1.0 to 2.5 MeV, subtract  $\phi_{In}$  from  $\phi_S$  (described in the next section).

#### Fast Flux Above 2.5 MeV

The sulfur (n,p) reaction can be used to relate the induced activity as measured by a GM-type counter to the incident fast neutron flux. The specific equation and pertinent constants follow:

$$\phi_S = FS = \frac{(CPMS)(QS)(CLFS)(SF)}{(WS)(K)(N_T)(\sigma_{eff})(1-e^{-\lambda T OS})(e^{-\lambda T1S})(60)} \text{ n/cm}^2/\text{sec,}$$

where, FS = sulfur measured flux - name used in computer code,

CPMS = sulfur count rate less GM counter background,

QS = counter efficiency factor at time of count = QC,

SF = factor changing QS to  $^{32}\text{P}$  calibration = 0.91 (ctr. A) and 0.837 (ctr. B),

CLFS = calibration factor for sulfur = 0.80 n/d,

WS = weight of 115 mils x 1/4 in D sulfur pellet = 0.260 g,

K = natural abundance of sulfur = 0.95,

$N_T = 1.88 \times 10^{22}$  nuclei/g,

$\sigma_{\text{eff}}$  = effective cross section =  $0.229 \times 10^{-24} \text{ cm}^2$ ,

TOS = exposure time in minutes,

TIS = time from exposure stop to mid-time of counting interval in minutes.

The equation simplifies to:

$$\phi_S = (3.26) \frac{(\text{CPMS})(\text{QS})(\text{SF})}{(\text{WS})(1-e^{-\lambda\text{TOS}})(e^{-\lambda\text{TIS}})} \text{ n/cm}^2/\text{sec.}$$

Supplying the unknowns to the simplified equations for each of the three materials enables the calculation of the fast neutron flux in the chosen energy range. A FORTRAN-IV computer code was found helpful for making the calculations. The KERMA in terms of millirad/hr can be calculated from  $\phi_{\text{Cu}}$ ,  $\phi_{\text{In}}$ , and  $\phi_S$  using the relation in Chapter II-C.

## LITERATURE CITED

1. Public Health Service. Medical Uses of Radium and Radium Substitutes. A Report on Conference held at The Center for Continuing Education, University of Chicago, September 3-4, 1964. Washington: U. S. Government Printing Office (1965).
2. "Prospects in Radiosurgery," Lancet 1 (7400) p. 1373 (1965).
3. E. E. Schwartz (ed.). The Biological Basis of Radiation Therapy. 1st ed., p. 327. Philadelphia: J. B. Lippincott Company (1966).
4. C. A. Tobias et al. "Radiological Use of High-energy Deuterons and Alpha-particles," Am. J. Roent. 67, p. 1 (1952).
5. S. Falkmer et al. "Pilot Study on Proton Irradiation of Human Carcinoma," Acta Radiol. 58 p. 33 (1962).
6. P. H. Fowler and D. H. Perkins. "The Possibility of Therapeutic Applications of Beams of Negative  $\pi$ -mesons," Nature 189 p. 524 (1961).
7. G. L. Locher. "Biological Effects and Therapeutic Possibilities of Neutrons," Am. J. of Roent. 36 (1) p. 1 (1936).
8. R. S. Stone. "Neutron Therapy and Specific Ionization," Am. J. Roent. 59 (6) p. 771 (1948).
9. J. O. Archambeau et al. "Neutron Symposium," Upton, N. Y. Report No. SM-44/20, IAEA. Vienna (1963).
10. R. G. Fairchild and L. J. Goodman. "Development and Dosimetry of an Epithermal Neutron Beam for Possible Use in Neutron Capture Therapy," Phys. Med. Biol. 11 (1) p. 15 (1966).
11. W. C. Reinig. "Advantages and Applications of  $^{252}\text{Cf}$  as a Neutron Source," (To be published) E. I. du Pont de Nemours and Company, Savannah River Laboratory (1968).

12. C. N. Wright et al. "Implantable Californium-252 Neutron Sources for Radiotherapy," Radiology 89 (2) p. 337 (1967).
13. J. J. Hazel. "Fast Neutrons for Radiation Therapy," Nucleonics 22 (11) p. 56 (1964).
14. J. F. Fowler and R. L. Morgan. "Pre-therapeutic Experiments with the Fast Neutron Beam from the Medical Research Council Cyclotron," Brit. J. Radiol. 36 (422) p. 121 (1963).
15. C. S. Schlea and D. H. Stoddard. "Californium Isotopes Proposed for Intracavity and Interstitial Radiation Therapy with Neutrons," Nature 206 (4988) p. 1058 (1965).
16. Ralston Paterson and H. M. Parker. "A Dosage System for Interstitial Radium Therapy," Brit. J. Radiol. 11 (124) p. 252 (1938).
17. U. S. Department of Commerce. National Bureau of Standards Handbook 87. Washington: U. S. Government Printing Office, p. 31 (1963).
18. U. S. Department of Commerce. National Bureau of Standards Handbook 85. Washington: U. S. Government Printing Office, p. 26 (1964).
19. G. N. Whyte. Principles of Radiation Dosimetry. 1st ed., p. 95. New York: John Wiley & Sons, Inc. (1959).
20. F. S. Williamson and Paul Mitacek, Jr. "Calculations of Kerma due to Fast Neutrons in Tissue-like Materials," Neutron Monitoring, Symposium Proceedings, Vienna, 1966, IAEA. Vienna p. 17 (1967).
21. Recommendations of the International Commission on Radiological Protection, Brit. J. Radiol. Suppl. 6 p. 25 (1955).
22. H. A. Bethe. "Nuclear Physics," Revs. Mod. Phy. 9 (2) p. 156 (1937).
23. R. C. Lawson, D. M. Clare, and D. E. Watt. "(D,D) and (D,T) Neutron Depth Dose Measurements in a Tissue-equivalent Phantom," Phys. Med. Biol. 12 (2) p. 201 (1967).

24. W. S. Snyder and J. Neufeld. "Calculated Depth Dose Curves in Tissue for Broad Beams of Fast Neutrons," Brit. J. Radiol. 28 (331) p. 342 (1955).
25. Gordon Kramer. "The Semiconductor Fast-neutron Dosimeter - Its Characteristics and Applications," IEEE Trans. on Nucl. Sci. 2, p. 106 (1966).
26. M. O. Thurston et al. "A Silicon Fast-neutron Dosimeter Having a Wide Sensitivity Range," Neutron Monitoring, Symposium Proceedings, Vienna, 1966, IAEA. Vienna p. 245 (1967).
27. B. H. Chase et al. "Development of a Fast Neutron Dosimetry System," Final Report No. COO-1226-12 to USAEC on Contract No. AT(11-1)-1226, from Phylatron Corporation. October (1966).
28. J. M. Swartz and M. O. Thurston. "Analysis of the Effect of Fast-Neutron Bombardment on the Current-Voltage Characteristic of a Conductivity-Modulated p-i-n Diode," J. of Apl. Phy. 37 (2) p. 745 (1966).
29. R. R. Speers. "Silicon Diode Fast-Neutron Dosimeter, Phase IV, Determination of the Energy Dependence of the Damage Constant," NDL-TR-83-IV. Nuclear Defense Laboratory (1967).
30. J. M. Swartz et al. "Silicon Diode Fast Neutron Dosimeter, Phase II, Isochronal and Isothermal Anneals of the Radiation Damage," NDL-TR-83-II. Nuclear Defense Laboratory (1967).
31. C. C. Gamertsfelder et al. "Some Notes on Practical Neutron Dosimetry," Neutron Dosimetry, Symposium Proceedings, Harwell, England, 1962, IAEA. Vienna p. 109 (1963).
32. D. J. Hughes. Pile Neutron Research. 1st ed., Ch. 4. Cambridge: Addison-Wesley Publishing Company (1953).
33. G. S. Hurst et al. "Techniques of Measuring Neutron Spectra with Threshold Detectors - Tissue Dose Determination," Rev. Sci. Instr. 27 (3) p. 153 (1956).
34. G. C. Robinson. "Neutron Dosimetry in Radiation-Damage Studies of Steel," Nuclear Safety 8 (4) p. 370 (1967).

35. G. D. Cola and A. Rota. "Calculation of Differential Fast-Neutron Spectra from Threshold-Foil Activation Data by Least Squares Series Expansion Methods," Nucl. Sci. Engr. 23 p. 344 (1965).
36. P. W. Reinhardt and F. J. Davis. "Improvements in the Threshold Detector Method of Fast Neutron Dosimetry," Hlth. Phy. 1 (2) p. 169 (1958).
37. K. C. Humpherys. "Some Neutron Dosimetry Standardization Efforts," Neutron Dosimetry, 2, Symposium Proceedings, Harwell, England, 1962, IAEA. Vienna p. 487 (1963).
38. C. N. Wright et al. "Savannah River Plant Criticality Dosimetry System," USAEC Report DP-1006. E. I. du Pont de Nemours and Company, Savannah River Laboratory (1960).
39. L. L. Anderson. "Cross Section of Copper-63 for Nuclear Accident Dosimetry," Hlth. Phy. 10 (5) p. 315 (1964).
40. A. M. Bresesti et al. "Threshold Detector Cross-Section Intercalibration in a Pure Fission Spectrum" Nucl. Sci. Engr. 29 (1) p. 7 (1967).
41. W. S. Snyder and J. Neufeld. "Calculated Depth Dose Curves in Tissue for Broad Beams of Fast Neutrons," Brit. J. Radiol. 33 (331) p. 342 (1955).
42. A. R. Boulogne and A. G. Evans. Personal communication, Savannah River Laboratory. Summer (1967).
43. C. N. Wright et al. "Implantable Californium-252 Neutron Sources for Radiotherapy," Radiology 89 (2) p. 337 (1967).
44. A. B. Smith and P. R. Fields. "Spontaneous Fission Neutron Spectrum of Cf<sup>252</sup>," Phy. Rev. 108 (2) p. 411 (1957).
45. P. R. Fields and Herbert Diamond. "Californium-252, A Primary Standard for Neutrons," Neutron Dosimetry, Symposium Proceedings, Harwell, 1962, IAEA. Vienna p. 581 (1963).
46. J. A. Auxier. "Multilaboratory Intercomparison of Neutron Dosimetry Systems," Neutron Monitoring, Symposium Proceedings, Vienna, 1966, IAEA. Vienna p. 625 (1967).

47. J. A. Auxier. "The Health Physics Research Reactor," Health Physics 11 (2) p. 89 (1965).
48. J. A. Auxier. "Radiation Dosimetry," Health Physics Division Annual Progress Report for Period Ending July 31, 1965, USAEC Report ORNL-3849. Oak Ridge National Laboratory (1966).
49. D. R. Johnson and J. W. Poston. "Radiation Dosimetry Studies at the Health Physics Research Reactor," USAEC Report ORNL-4113. Oak Ridge National Laboratory (1967).
50. Lawrence Dresner. Principles of Radiation Protection Engineering. 1st ed., p. 109. New York: McGraw-Hill (1965).
51. Henry Margenau. The Mathematics of Physics and Chemistry. 2nd ed., p. 479. Princeton: Van Nostrand (1956).
52. T. A. Barr and G. S. Hurst. "Fast-Neutron Dose in a Large Tissue-Equivalent Phantom," Nucl. 12 (8) p. 33 (1954).
53. S. B. Field and C. J. Parnell. "The Use of Threshold Detectors to Determine Changes in a Fast Neutron Energy Spectrum with Depth in a Phantom," Brit. J. Radiol. 38 (452) p. 618 (1965).
54. E. P. Vega. "Evaluation of the Response of Silicon Diode Dosimeters to Fast Neutrons," NDL-TM-31. Nuclear Defense Laboratory (1967).